(7)

THE ROLE OF NUCLEI SIZE IN TRANSIENT CAVITATION THRESHOLD MEASUREMENTS

THE UNIVERSITY OF MISSISSIPPI
PHYSICAL ACOUSTICS RESEARCH GROUP
DEPARTMENT OF PHYSICS AND ASTRONOMY

(7)

Approved for Public Release: Distribution Unlimited

Technical Report for
Office of Naval Research
Contract N00014-84-C-0193

THE ROLE OF NUCLEI SIZE IN

TRANSIENT CAVITATION THRESHOLD MEASUREMENTS

by

R. A. Roy* and L. A. Crum
Physical Acoustics Research Laboratory
The University of Mississippi
University, MS 38677

Sept. 1, 1984

*MS Thesis directed by L. A. Crum

Unclassified

SECURITY CLASSIFICATION OF THIS PAGE (When Data Entered)

REPORT DOCUMENTATION PAGE	READ INSTRUCTIONS BEFORE COMPLETING FORM
1. REPORT NUMBER: 2-84	2. GOVT ACCESSION NO.: AD-A148334
3. RECIPIENT'S CATALOG NUMBER	
4. TITLE (and Subtitle): The Role of Nuclei Size in Transient Cavitation Threshold Measurements	5. TYPE OF REPORT & PERIOD COVERED: Technical
	6. PERFORMING ORG. REPORT NUMBER
7. AUTHOR(s): R. A. Roy and L. A. Crum	8. CONTRACT OR GRANT NUMBER(s): N00014-84-C-0193
9. PERFORMING ORGANIZATION NAME AND ADDRESS: Physical Acoustics Research Laboratory, Department of Physics, University of Miss., University, MS 38677	10. PROGRAM ELEMENT, PROJECT, TASK AREA & WORK UNIT NUMBERS
11. CONTROLLING OFFICE NAME AND ADDRESS: Office of Naval Research, Physics Div., Code 412, Arlington, VA 22217	12. REPORT DATE: 9-1-84
	13. NUMBER OF PAGES: 77
14. MONITORING AGENCY NAME & ADDRESS(if different from Controlling Office)	15. SECURITY CLASS. (of this report): Unclassified
	15a. DECLASSIFICATION/DOWNGRADING SCHEDULE

16. DISTRIBUTION STATEMENT (of this Report)

Approved for public release; distribution unlimited

17. DISTRIBUTION STATEMENT (of the abstract entered in Block 20, if different from Report)

18. SUPPLEMENTARY NOTES

19. KEY WORDS (Continue on reverse side if necessary and identify by block number)

Cavitation
Nuclei
Nonlinear Oscillations
Bubbles

20. ABSTRACT (Continue on reverse side if necessary and identify by block number)

The relationship between cavitation nuclei size and transient cavitation thresholds was studied employing an apparatus designed to perform automated threshold measurements using sound emission and sonoluminescence as transient cavitation indicators. Experimental results agree with crevice model predictions for larger nuclei sizes. However, for nuclei radii smaller than about 5μ, experimental thresholds are higher than theoretical predictions based on either the crevice or free bubble nucleation models. Observed deviations

DD FORM 1 JAN 73 1473 EDITION OF 1 NOV 65 IS OBSOLETE

S/N 0102-LF-014-6601

Unclassified

SECURITY CLASSIFICATION OF THIS PAGE (When Data Entered)

may be due to limitations in the theories or systematic experimental errors.

ACKNOWLEDGEMENTS

I am very grateful to professors Lawrence A. Crum and James J. Reidy, my thesis advisors, for their encouragement and advice throughout the course of this project. I am particularly indebted to Timothy Farris and Brian Fowlkes for their invaluable assistance in the lab. I also benefited from conversations with Anthony Atchley, Gary Hansen and Robert Apfel, Professor of Applied Mechanics at Yale University. Most of all I would like to thank my wife, Nancy, for her patience and loving support and my good friend Michael for simply being there. This work was supported by the National Science Foundation and the Office of Naval Research.

TABLE OF CONTENTS

LIST OF TABLES vi
LIST OF FIGURES vii

Chapter page

1. INTRODUCTION 1

Survey of Nucleation Models 2
Stabilized Nuclei 3
Stabilized Free Microbubbles 3
The Crevice Model 5
Radiation Induced Nucleation 6
Transient Cavitation 7
A Restatement of Objectives 9
A Brief Description of the Apparatus 9

2. THEORETICAL CONSIDERATIONS 11

Transient Cavitation Thresholds 11
Free Bubble Thresholds 12
Crevice Model Thresholds 18
Sonoluminescence 22

3. EXPERIMENTAL APPARATUS 25

The Resonance Sphere and PMT Assembly 25
The Fluid Management System 27
Materials Used 27
Temperature Control 28
Surface Tension Measurement 29
Control of Gas Concentration 29
Control of Nuclei Size 30
The System Electronics 31
The Acoustical Power and Frequency Control System . . . 31
The Gating, Triggering and Timing Circuitry 32
System Calibration 35

4. EXPERIMENTAL PROCEDURE 37

Sample Preparation 37
Data Acquisition 38

5. RESULTS AND CONCLUSIONS 41

Experimental Results 41
Relationship Between Theory and Experiment 43
Free Bubble Model 43
Crevice Model 45
Experimental Uncertainties 46
The Question of Sonoluminescence 48
Instrument Improvement 49
Concluding Remarks 51

BIBLIOGRAPHY 53

APPENDIX 55

BIOGRAPHICAL SKETCH OF THE AUTHOR 77

LIST OF TABLES

Tables		page
I	The Effect of Thermal Conductivity on Sonoluminescent Intensity	23
II	Experimental Parameters	40
III	Experimental Results	42
IV	Experimental Uncertainties	46

LIST OF FIGURES

Figure		page
I	Free Gas Bubble in a Liquid	56
II	Gas Stabilized in a Crevice	56
III	Simplified Experimental Arrangement	57
IV	Blake Thresholds	58
V	Free Bubble Thresholds	59
VI	Illustrated Growth Times	60
VII	Modified Free Bubble Thresholds	60
VIII	Critical Crevice	61
IX	Noncritical Crevices	61
X	Nucleating Bubble	61
XI	Resonance Cell/Photomultiplier Tube Assembly	62
XII	Photograph of the Resonance Cell	63
XIII	Photograph of the Resonance Cell/PMT Assembly	63
XIV	Axial Field Survey	64
XV	Fluid Management System	65
XVI	Photograph of the Filtration System	66
XVII	Photograph of the Gassing/Degassing System	66
XVIII	Temperature Monitoring System	67

Figure page

XIX Photograph of the Tensiometer 68

XX Photograph of the Van Slyke Apparatus 68

XXI Photographs of the System Electronics 69

XXII Acoustical Power and Frequency Control Circuitry 70

XXIII Gating, Triggering and Timing Circuitry 71

XXIV Timing Characteristics 72

XXV Noise Gating Network 73

XXVI Relationship Between Primary and Secondary Pressure Maxima 74

XXVII System Calibration Curve 74

XXVIII Sample Strip Chart Record 75

XXIX Experimental Results 76

Chapter 1

INTRODUCTION

A fundamental problem in the study of cavitation phenomena is one of understanding the conditions required for its onset. For liquids, a determination of these conditions is tantamount to measuring the liquid's tensile strength. Laboratory measurements of the tensile strength of water have yielded values (e.g. 5 Bars) that are significantly less than predictions based on homogeneous nucleation theory (~1000 Bars). The reduced strength is attributed to the existence of local inhomogeneities within the bulk of the fluid. These "weak spots" serve as preferential sites for the onset of liquid rupture. For the purpose of this study, such inhomogeneities are referred to as nuclei and the term cavitation is defined as the expansion of a preexisting nucleus to a size where macroscopic effects become observable.

Liquid tensile strengths may be obtained by measuring the minimum negative acoustic pressure required to initiate cavitation. This negative pressure is called the acoustic cavitation threshold of the liquid. Such thresholds depend on several parameters, such as: the physical properties of the liquid, the static pressure, the frequency of the sound field, and the characteristics of the nuclei themselves. The

purpose of this experiment was to investigate the cavitation threshold of water as a function of nuclei size, all other factors held constant.

1.1 Survey of Nucleation Models

The most obvious model for a nucleus, illustrated by Figure I, is that of a small gas bubble in a liquid. The condition for mechanical equilibrium at the microbubble wall is

$$[P_g+P_v]-P_h = 2\sigma/R \quad , \tag{1}$$

where P_g is the gas pressure, P_v is the vapor pressure, P_h is the hydrostatic pressure, R is the bubble radius and σ is the surface tension. For a gas filled bubble, Henry's law maintains that the nuclei will not dissolve if

$$P_g+P_v = P_o \quad , \tag{2}$$

where P_o is the external ambient pressure. Accordingly, a gas and vapor filled bubble will be stable only if the hydrostatic pressure is below the ambient pressure by the amount $2\sigma/R$. However, unless the liquid is artifically stressed, either statically or hydrodynamically, the hydrostatic pressure is greater than the ambient pressure. Thus, assuming a permeable cavity wall, the bubble will dissolve. Epstein and Plesset [1] maintained that bubbles of the order of a few microns in diameter will dissolve in a few seconds. Large bubbles last longer, but

buoyancy forces drive them to the surface. Consequently, there must exist a mechanism by which these bubbles are stabilized from dissolution. Such stable gas pockets are referred to as stabilized nuclei.

1.1.1 Stabilized Nuclei

Several models, none of which is firmly established, have been proposed as possible stabilization mechanisms. We briefly describe the more accepted ones, which are subdivided into two categories: (1) stabilized free bubbles and (2) gas pockets stabilized in crevices.

1.1.1.1 Stabilized Free Microbubbles

Fox and Hertzfeld [2] proposed that microbubbles may be stabilized by rigid, impermeable organic skins that mechanically prevent the loss of gas by diffusion. Cavitation occurs when the skin breaks, the threshold determined by the strength of the film and the size of the bubble. Conversely, these skins can be crushed by an increase in hydrostatic pressure. Fox and Hertzfeld predicted a linear dependence between hydrostatic pressure and cavitation threshold up to the point where the skin crushes and the nuclei rapidly dissolve, thus increasing the cavitation threshold dramatically. However, Strasberg [3] has shown that cavitation thresholds in water smoothly increase with hydrostatic pressure, a result that prompted Hertzfeld to abandon the model.

Yount [4] expanded upon this theme by proposing that stabilization results from surface active skins of varying permeability. These skins, which are initially gas permeable, become impermeable when the surface molecules are forced closer together as the bubble contracts. Outgassing is therefore arrested and the microbubble stabilizes at some critical radius. The condition for mechanical equilibrium becomes

$$[P_g+P_v] - P_h = [2\sigma/R] - [2\Gamma(R)/R] \quad , \tag{3}$$

where the second term on the right is called the "skin pressure". Yount maintained that one may consider the skin compression, Γ, as effectively reducing the surface tension. Yount's theory is a complex, multiparameter treatment that has sucessfully predicted bubble counts in supersaturated gelatin [5] and modeled decompression sickness in divers [6].

In 1894, Thompson [7] observed the existence of negative charges on air bubbles in water. Further work by McTaggort [8] and Alty [9] indicated that the magnitude of the charge is independent of the nature of the gas and increases with increasing electrical conductivity of the water. Alty [10] proposed that the origin of the charge was due to selective absorption of ions from the water onto the bubble surface. Inspired by this work, Akulichev [11] proposed a model by which microbubbles are stabilized by coulomb repulsion of surface active ions.

He found that the cavitation threshold of water was in fact reduced by the addition of hydrophobic ions such as CL^- and F^-. Syrotyuk [12], on the other hand, observed essentially no variation in threshold with electrical conductivity. It appears that the experimental evidence pertaining to this mechanism is ambiguous at best.

1.1.1.2 The Crevice Model

One of the most extensively studied schemes proposed for nuclei stabilization results from the work of Harvey and others [13] in which gas is trapped in a conical crevice of an imperfectly wetted dirt particle (mote) present in the liquid. This configuration, illustrated in Figure II, is stable if the pressure is balanced across the gas-liquid interface. This is indeed the case provided the interface is concave outward so that the surface tension serves to balance the hydrostatic and ambient pressures. Mechanical equilibrium occurs when

$$P_h - [P_g + P_v] = 2\sigma/R \quad . \tag{4}$$

For small R, the term on the right can become quite large; thus, one can see that even for large applied hydrostatic pressures, some crevices can stabilize gas. Evidence in favor of the crevice model is provided by Greenspan and Tschiegg [14] who observed that the cavitation threshold of water increased from less than 1 Bar to more than 150 Bars following protracted filtration. Winterton [15] successfully applied the crevice

model to the study of nucleation in boiling. The theory has been extended by Strasberg [16], Apfel [17], and Crum [18].

1.1.2 Radiation Induced Nucleation

It is now appropriate to consider the process by which the nuclei are created so that they can be subsequently stabilized. Note that with the exception of the crevice model, all the stabilization schemes discussed thus far require such a production mechanism. The commonly accepted model considers the interaction of ionizing radiation with the liquid, thus creating localized "hot spots" due to the deposition of the particle energy into the fluid. Liberman [19] irradiated pentane and acetone with a flux of fast neutrons from a Po-Be source and found that the acoustic cavitation threshold fell by an order of magnitude. Greenspan and Tschiegg [14] irradiated a sample of "clean" water with 10-MeV neutrons and observed the threshold drop from 150 Bars to about 50 Bars. Greenspan noted that in order to observe some cavitation threshold (P_t) due to irradiation from a source, one must first remove from the liquid all the stabilized nuclei which cavitate at acoustic pressure amplitudes less than about $2P_t$. For water, Greenspan found it necessary to subject his samples to protracted filtration through a 0.2 micron filter. The water samples studied in this thesis are not nearly as clean. One concludes that radiation induced nucleation, although undoubtedly occurring, should not affect our threshold measurements and thus will not draw consideration as an influential nucleation mechanism.

1.2 Transient Cavitation

Up to this point, the term "cavitation" has referred to the expansion of a preexisting nucleus to a size where macroscopic effects take place. When such an expansion is initiated by an acoustically generated stress, the behavior is labeled "acoustic cavitation". In this experiment, water was dynamically stressed by a spherically symmetrical stationary acoustic field. For very large peak negative pressures, the water ruptures and a rapidly growing vapor cavity is formed which subsequently undergoes a violent collapse during the ensuing positive pressure cycle (some might survive a cycle or two). Such behavior is termed "transient acoustic cavitation" and the minimum acoustic pressure amplitude necessary to initiate such an event is called the transient acoustic cavitation "threshold". For our purposes, all cavitation phenomena is acoustically generated, thus the label will be suppressed.

When a transient cavity collapses, a number of macroscopic effects take place. The task of establishing the existence of transient cavitiation activity corresponds to that of detecting one or more of the resulting effects. Violent collapses generate shock waves that propagate through the liquid resulting in audible "clicks" or "pings" (a consequence of bubble wall velocities that exceed the velocity of sound in the fluid and their resultant interaction with the boundries of the

cavitation cell). In standing wave acoustic systems, such shocks reduce the Q of the system and therefore the output amplitude (from a hydrophone) as well. The temperatures and pressures at the collapse point reach several thousand degrees and atmospheres respectively. These extreme conditions incandesce the gas in the bubble, which results in light emission, a process known as "sonoluminescence".

The definition of what constitutes the transient cavitation threshold is quite arbitrary. Crum [20] defines the transient cavitation threshold as the minimum acoustic pressure amplitude required to initiate an audible click in a standing wave system. Greenspan and Tschiegg [14] choose to regard the threshold as the "negative pressure below which cavitation is rare". For purposes of this study, we adopt Crum's definition of threshold but we also consider the threshold for sonoluminescence emission. The prior definition establishes a condition on the bubble wall velocities whereas the latter presumably establishes a condition on the collapse temperatures. The encoding of cavitation information in optical form permits one to take advantage of the broad range of instrumentation (i.e. discriminators, coincidence units, etc.) designed to operate with modern photodetectors. This paper is in part a feasibility study of such a detection scheme.

1.3 A Restatement of Objectives

Armed with some background information, we shall now restate the objective of this investigation. We aspire to gain insight into the nature of cavitation nuclei. As we shall see, the stabilized free bubble models predict transient cavitation thresholds that are proportional to $R_o^{6/5}$ (R_o is the radius of the stabilized microbubble) for large nuclei and are inversely proportional to R_o for small bubbles. On the other hand, the crevice model exhibits no explicit dependence of threshold with mote size for the range of sizes under study. Thus inspired, our main objective is to determine experimentally the relationship between nuclei size and the transient cavitation threshold of water. In the process we hope to establish the feasibility of automated threshold measurements using sonoluminescence as the cavitation indicator.

1.4 A Brief Description of the Apparatus

Since, in this experiment, we are concerned with the relative change in threshold with nuclei size, it is just as important that we establish consistency in sample preparation and measurement technique from one run to another than it is that we establish absolute accuracy in threshold measurements. Our goal is to design an apparatus that performs threshold measurements in an automated and reproducible fashion.

Figure III is a simplified diagram of such a device. The spherical quartz resonator which contains a suitably prepared sample of water is housed in a light-tight enclosure along with a condenser microphone and a photomultiplier tube (PMT). The sound pressure level in the resonator is gradually increased until a transient cavitation event takes place. The resulting audible click is normally accompanied by a sonoluminescence flash that generates an electrical pulse at the anode of the PMT base. After appropriate gating and discrimination, this pulse activates a circuit that switches off the sound field for a predetermined length of time, a process that is hereafter referred to as "automatic triggering". If light emission does not occur soon after an audible click is heard the operator manually activates the trigger circuitry, a process we refer to as "manual triggering". Whether manual or automatic, the above sequence of events constitutes a threshold measurement and is automatically repeated as often as the operator chooses. This results in a series of cavitation threshold determinations that yield a mean threshold for a particular set of fluid parameters. The closed fluid flow system facilitates the control and monitoring of various fluid properties such as temperature, dissolved gas content, surface tension, and nuclei size. A more detailed description of the above systems follows in chapter three.

Chapter 2

THEORETICAL CONSIDERATIONS

In this section we focus upon the theoretical aspects of this investigation. Transient cavitation thresholds are presented, followed by a qualitative discussion of the sonoluminescence phenomena. Since this is not a major portion of this study, the reader is referred to previously published articles: [21], [22], [23], [17], [18].

2.1 Transient Cavitation Thresholds

We aspire to determine theoretically the manner in which cavitation thresholds vary with nuclei size (free bubble radius or mote diameter). Ideally, such a theory should incorporate the effects of the stabilizing mechanism as well as the bubble dynamics. Collapse velocities for transient cavities approach the speed of sound in the liquid. We therefore assume that in the case of stabilized free bubbles, the bubble wall velocities are so great that any contributions to bubble dynamics from a stabilization mechanism is negligible. The crevice model, in which the cavitation threshold is essentially the threshold for nucleating a free bubble from a crack in a mote, is a somewhat different situation and is treated separately.

2.1.1 Free Bubble Thresholds

Blake [21] was one of the first to consider the theoretical aspects of acoustic cavitation inception. Assuming that air bubbles exist in mechanical equilibrium with their surroundings, he determined the condition for cavitation inception to be:

$$P_b = P_o + (4/3)\left[\frac{2\sigma^3}{3R_o^3(P_o+2\sigma/R)}\right]^{\frac{1}{2}} . \qquad (5)$$

In this equation, P_b is the threshold acoustic pressure, R_o is the initial bubble radius, P_o is the ambient pressure and σ is the surface tension. This "Blake threshold" corresponds to the minimum acoustic pressure at which a bubble of radius R_o *begins to grow*. His is a static theory that serves as a condition for bubble nucleation (mechanical growth).

Apfel [22] has recently developed a theory that includes dynamic effects, taking into account the fact that time is needed for bubble growth. By neglecting the contributions of surface tension, viscosity, and inertia he makes a crude analytical estimate of the maximum radius to which a bubble can grow, given the ambient pressure, the acoustic pressure amplitude and the density of the liquid. He considers the pressure external to the bubble as being composed of a static part P_o and a time varying part P(t). Assuming the negative half-cycle comes first, he writes $P(t)=-P_a \sin\omega t$ where P_a is the acoustic pressure

amplitude. Neglecting the contribution of the bubble's internal gas pressure, which falls rapidly during bubble growth, Apfel writes the pressure difference across the bubble wall ($P_{int} - P_{ext}$) as

$$\delta P = P_a \sin\omega t - P_o \quad , \tag{6}$$

where ω is the frequency and P_o is the ambient pressure. The growth is considered to occur in two stages:

(i) During the interval, T_g, for which δP is positive, the liquid is in tension and the bubble grows to some radius R_1. The average bubble wall velocity is approximately

$$V = (2\Delta P/3\rho)^{\frac{1}{2}} \quad , \tag{7}$$

where ρ is the fluid density and $\Delta P = <\delta P>$ is the time averaged pressure difference during the growth stage. Apfel derives approximate values for T_g and ΔP by considering a Taylor expansion of the pressure difference about $\omega t = \pi/2$, the point of maximum tension. His results, to second order, are

$$T_g = (2/\omega)\left[\frac{2(\zeta-1)}{\zeta}\right]^{\frac{1}{2}} \quad , \tag{8}$$

and

$$\Delta P = (2/3)P_o[\zeta-1] \quad , \tag{9}$$

where

$$\zeta = P_a/P_o \quad . \tag{10}$$

The bubble radius at the end of this first stage is therefore given by

$$R_1 = VT_g = (4/3\omega)(\zeta-1)\left[\frac{2P_o}{\rho\zeta}\right]^{1/2} . \qquad (11)$$

(ii) As the pressure difference goes negative, the bubble continues to grow due to its outward momentum, thus we now consider the period from the time δP becomes negative to the point where the bubble wall momentum goes to zero. Assuming that $\delta P=-P_o$ for this interval, we equate the initial kinetic energy of the fluid surrounding the bubble to the increase in potential energy of its contents as the bubble expands to its maximum radius, R_m. This results in

$$R_m = (4/3\omega)(\zeta-1)(2P_o/\zeta\rho)^{1/2}[1+(2/3)(\zeta-1)]^{1/3} , \qquad (12)$$

which is the maximum radius a bubble can grow to in a liquid of density ρ at ambient pressure P_o while stressed by an acoustic field of pressure amplitude P_a.

Apfel goes on to demonstrate that despite its approximate nature, eq. (12) does, in fact, generate bubble growth values that are in reasonable agreement with much more complicated numerical solutions [23] of the differential equations that govern bubble dynamics. Note also that R_m is independent of R_o; thus, for a particular sound field and liquid, all the bubbles grow to the same maximum radius regardless of the original size provided P_a exceeds the Blake threshold for a particular R_o. To

illustrate this concept, consider a distribution of microbubbles in water stressed by 50kHz acoustic field of pressure amplitude 1.25 Bars. From eq. (12), one calculates R_m to be 14μ. Next, consider a plot of the Blake threshold for bubbles in water as illustrated by Figure IV. Although eq. (12) maintains that all these bubbles expand to a radius of 14μ, Blake's theory insists that only bubbles larger than approximately 2μ will grow at all. For a given acoustic pressure amplitude and initial bubble radius, one must first be assured of nucleation ($P_a > P_b$) before considering the dynamics of bubble motion.

Suitably forewarned, we proceed to derive an expression for the transient cavitation threshold. Drawing from the work of Neppiras and Noltingk, Apfel utilizes the following criteria for a transient cavity:

$$R_m/R_o = 2.3 \quad , \tag{13}$$

which corresponds to the point where the bubble collapse velocity equals the speed of sound in the liquid, in the incompressible assumption. Therefore, at threshold we let

$$P_a = P_t \quad , \quad \zeta_t = P_t/P_o \quad , \text{ and } \quad R_m = 2.3R_o \quad , \tag{14}$$

where P_t is the threshold acoustic pressure amplitude. Eq. (12) becomes

$$R_o = (.82/\omega)(\zeta_t - 1)(P_o/\rho\zeta_t)^{\frac{1}{2}}[1+(2/3)(\zeta_t - 1)]^{1/3} \quad . \tag{15}$$

Figure V is a plot of P_b and P_t vs. R_o over a spread of nuclei sizes ranging from 0.5μ to 40μ. One is tempted to say that, for $R_o > 2.75\mu$, the

transient threshold (P_t) applies whereas for smaller bubbles the Blake threshold prevails. However, the situation is not this simple. Consider the scenerio proposed by Figure VI, where we have a 1μ bubble subject to an acoustic pressure amplitude slightly larger than P_b. The conditions for both nucleation and transient cavitation are met, but the bubble may not evolve to its transient state because there exists a limited time, ΔT, for growth to take place. We write this growth time as

$$\Delta T = (\tau/2) - (2T_b) \tag{16}$$

where τ is the acoustic period and T_b is the point in time at which the acoustic pressure equals the Blake pressure. Therefore,

$$P_a \sin(\omega T_b) = P_b$$

and (17)

$$\Delta T = (1/\omega)[\pi - 2\arcsin(P_b/P_a)] \quad .$$

Returning to the derivation of eq. (12), one can generate an approximate correction for R_m by choosing ΔT (rather than T_g) to be the time available for bubble growth and assuming that the time averaged pressure difference, ΔP, remains unchanged. After substituting eq. (17) in place of eq. (8), one arrives at

$$R_m' = (2/3\omega)\left[\frac{P_o(\zeta'-1)}{\rho}\right]^{\frac{1}{2}}[\pi - 2\arcsin(P_b/P_a')][1+(2/3)(\zeta'-1)]^{1/3} \tag{18}$$

where the ' is introduced to avoid confusion with the previous result.

Note that, unlike R_m, R_m' is a function of R_o via its explicit dependence on the Blake threshold. To generate a P_t' vs. R_o curve using eq. (18) we employ an iterative approach where, for a given R_o, we calculate the Blake threshold and insert this value into eq. (18). Using a computer, we increment P_a' until $R_m'=2.3R_o$, which yields the threshold pressure, P_t', for a particular bubble radius. The results of such a procedure are plotted as the broken curve in Figure V. Note the close agreement with previous theories thereby suggesting that, for small bubbles, the limitation placed on available growth time is more or less offset by increased growth rates (larger ΔP in eq. (7)) and the fact that small bubbles do not need to grow much in order to be considered transient cavities. The P_t' curve dips below P_t as R_o increases because, as P_b approaches P_o, ΔT does not go to T_g but is actually a few percent larger. For the range of nuclei under study ($0.5\mu<R_o<10\mu$) this distinction lies well within the limits of experimental uncertainty.

In its present form, the P_t' vs. R_o curve is not directly applicable to this particular experiment, in that we control nuclei size by filtering the water in a closed circulation system. Thus we place only an upper bound on the nuclei size distribution, whereas the 2.5μ nuclei have the lowest threshold and therefore cavitate first. Figure VII provides a suitably modified free bubble threshold curve drawn over the range of nuclei sizes encountered in this experiment.

2.1.2 Crevice Model Thresholds

Imperfectly wetted microscopic crevices in motes provide ideal sites for small pockets of gas to be trapped. Harvey [13], Apfel [17], Crum [18] and others have developed a simple scheme for describing the way that gas stabilizes in these cracks. Figure VIII depicts an imperfectly wetted conical crevice in a mote. The stabilization condition for this system is

$$P_h = P_v + P_g + (2\sigma/R) \quad , \tag{19}$$

where P_h is the hydrostatic pressure, P_v is the liquid vapor pressure, P_g is the equilibrium gas pressure, σ is the surface tension and R is the equilibrium radius of curvature of the liquid-gas interface. Eq. (19) determines the final position of the interface in the crevice. Increasing the hydrostatic pressure increases the radius of curvature until the angle between the interface and the crack wall reaches a maximum value, α_a, known as the advancing contact angle. This situation, which is illustrated in Figure VIII is characteristic of what Apfel terms a crevice of "critical size". A further increase in P_h (or reduction in P_v or P_g) serves to drive the interface toward the apex whereas a reduction in hydrostatic pressure serves to reduce the angle of contact. These conditions can also be achieved by increasing or reducing the half-diameter at the mouth of the crevice, the prior resulting in a crack greater than critical size and the latter corresponding to a crevice size smaller than the critical value as shown

in Figure IX. The half-diameter, A_c, at the mouth of a critical crevice is given by

$$A_c = R|\cos(\alpha_a-\beta)| \quad , \tag{20}$$

Where β is the crevice angle. Substituting R from eq. (19) yields

$$A_c = \frac{2\sigma|\cos(\alpha_a-\beta)|}{(P_h-P_g-P_v)} \quad . \tag{21}$$

The introduction of an acoustic stress serves to reduce the liquid pressure and causes the interface to bow outward as shown in Figure X. A sufficient reduction will cause the receding contact angle, α_r, to be reached; the interface propagates outward and a transient cavity nucleates. Following a theory developed by Apfel [17] and others, one can determine the threshold acoustic pressure required to generate such an event. Apfel's expressions for the threshold pressure, P_{tc} are

$$P_{tc} = [P_h-\gamma P_g-P_v] + (P_h-P_g-P_v)\left|\frac{\cos(\alpha_r-\beta)}{\cos(\alpha_a-\beta)}\right| \quad , \tag{22}$$

for crevices larger than critical size and

$$P_{tc}' = [P_h-\gamma P_g-P_v] + (2\sigma/A_o)|\cos(\alpha_r-\beta)| \quad , \tag{23}$$

for cracks that are smaller than critical size. In the above expressions $\alpha_r>\beta$ and γ is a positive constant (less than or equal to one) that reflects the inability of the nucleating gas pocket to

maintain the equilibrium gas pressure due to the finite diffusion rates across the gas liquid interface. Crum [18] modified this theory by explicitly introducing the contribution of surface tension. He accomplished this by writing $\cos(\alpha_r-\beta)$ as

$$\cos(\alpha_r-\beta) = \cos(\alpha_e-[\alpha_h+\beta]) \quad , \tag{24}$$

where α_e is the equilibrium contact angle and α_h is the hysteresis between the equilibrium and the receding contact angles. Bargeman and Van Voorst Vader [24] write α_e as

$$\cos\alpha_e = (C/\sigma)-1 \quad , \tag{25}$$

thus permitting one to write equations (22) and (23) as

$$P_{tc} = [P_h-\gamma P_g-P_v] + \frac{(P_h-P_g-P_v)}{\delta}[\cos\theta(C/\sigma-1)+\sin\theta(1-(C/\sigma-1)^2)^{\frac{1}{2}}] \quad , \tag{26}$$

and

$$P_{tc}' = [P_h-\gamma P_g-P_v] + (2\sigma/A_o)[\cos\theta(C/\sigma-1)+\sin\theta(1-(C/\sigma-1)^2)^{\frac{1}{2}}] \quad , \tag{27}$$

where $\theta=\alpha_h+\beta$, $\delta=\cos(\alpha_a-\beta)$, σ is the surface tension and C is a constant that depends on the surface properties of the solid. For nonpolar solids, C~50 dynes/cm.

We now have expressions that permit us to calculate cavitation thresholds once the parameters δ, γ, and θ are specified. Experimenting with nonfiltered water, Crum [18] varied these quantities in such a way as to provide a best fit of eq. (24) to his measured results. He found

a set of values that not only lay within the range of previously measured results [25] [26] but also provided a good fit to data for a variety of gas pressures, surface tensions and temperatures. Brosey [27] adopted a similar process and found the same three values (as Crum) yielding the best fit to his data. Since the source for the water used in this experiment was the same as that used by both Crum and Brosey, it seems reasonable to assume that the nature of the motes would be similar. Thus, for purposes of this investigation, we assume, as did Crum and Brosey, that $\alpha_a=106^0$, $\beta=14^0$, $\alpha_h=18^0$ and $\gamma=1$.

Note that eq. (24) is not dependent on the size (diameter) of the crevice whereas eq. (25) has the threshold increasing with decreasing A_o. In this experiment we operate at a hydrostatic pressure of 1 Bar, a gas pressure of 0.5 Bar and a vapor pressure of 0.027 Bar. Substituting these along with the previously specified crack and contact angle into eq. (21) gives a critical crevice half-diameter of 0.11μ. We assume that A_c is roughly 1/5 of the mote diameter, which yields a critical mote size of about 0.5μ. The smallest filter pore size employed in this experiment is 1μ, thus the smallest motes are all larger than critical size and we expect the threshold to be relatively independent of filter size. Using the parameters presented above, one calculates the transient cavitation threshold pressure to be 3.8 Bars.

2.2 Sonoluminescence

As stated previously, collapsing transient cavities generate temperatures and pressures at the collapse point that are intense enough to induce light emission. The exact nature of this process is not firmly established but most investigators believe that the sonoluminescence is thermal in origin, resulting from either the incandescence of hot gas and/or thermal dissociation and recombination of reactive chemical species. Regardless of specific origin, it is useful to know how to maximize the light output and thereby increase the effectiveness of sonoluminescence as a cavitation indicator.

Jarman [28] found that the light intensity decreased with increasing liquid temperature. He also found that alcohols emit less light than water. Both of these results are attributable to the fact that increasing the vapor pressure serves to dampen the cavity collapse.

Low viscosity fluids undergo violent collapse more readily and thus emit more light. However, viscous fluids may experience large amplitude radial oscillations that sonoluminesce. Although rare, such stable cavities have been observed by Saksena and Nyborg [29].

Prudhomme and Guilmart [30] observed that the relative intensity of emitted light varied inversly with the thermal conductivity of the dissolved gas. Their results are reproduced below in table I, where Ω

is the thermal conductivity in units of (cal/cm/sec/^{0}C)x10^3. Although enhanced thermal conduction may increase collapse velocities, the collapse temperatures are none the less reduced. It appears that adiabatic collapses are preferable.

Dissolved Gas	Ω	Relative Intensity
Xenon	.0124	540
Krypton	.0212	180
Argon	.0385	54
Nitrogen	.055	45
Oxygen	.0583	35
Neon	.1092	18
Helium	.3365	1
Hydrogen	.414	--

TABLE I

Sirotyuk and Rosenberg [31] observed that increasing the acoustic pressure amplitude enhances the measured light output, presumably because of increased collapse velocities generating higher temperatures. Thus, raising the transient cavitation threshold pressure should improve the effectiveness of sonoluminescence as a transient cavitation indicator. One way to raise the threshold is to reduce the dissolved gas content, thereby reducing P_g. However, the quantity of light emitted is also proportional to the amount of gas available to incandesce/react and thus a tradeoff exists.

We found (quite empirically) that, using Argon as the dissolved gas, our best results occurred at a gas pressure of about 0.5 Bar.

One can also enhance light output via the addition of chemiluminescent compounds to the liquid. According to several investigators, the addition of sodium luminol increases light output dramatically [28]. Since the chemistry of the liquid is critical in nuclei stabilization studies, the addition of such agents is not attempted here.

To this point, nothing has been said concerning the relationship between transient cavitation thresholds determined via sonoluminescence and thresholds detected audibly. Although one can actually calculate collapse temperatures, this information is of limited usefulness because we do not know the minimum temperatures and pressures needed to generate light. Previous experience tells us that the two thresholds coincide, at least for larger nuclei. However, collapse temperatures are roughly proportional to R_m which, according to eq. (13), decreases with decreasing nuclei size. Also, smaller bubbles (as well as cracks in smaller motes) contain less gas. Therefore an increase in the "sonoluminescence threshold" for smaller filter sizes would come as no surprise. Whether or not this occurs remains to be seen. For a more detailed and quantitative discussion of the sonoluminescence phenomena, the reader is referred to two excellent review articles by Finch [32] and Flynn [33].

Chapter 3

EXPERIMENTAL APPARATUS

In this chapter we present a detailed description of the experimental apparatus. The discussion is subdivided into four sections:

(A) The resonance sphere and PMT assembly,

(B) The fluid management system,

(C) The system electronics,

(D) System Calibration.

3.1 The Resonance Sphere and PMT Assembly

Figure XI illustrates the fused quartz resonance sphere (or "cell") used to generate the acoustic standing wave. It has a volume of one liter, a neck i.d. of 1.00cm, a neck o.d. of 1.31cm, a neck length of 5.9cm and a 4cm diameter flat on the base. Vibrational excitation is provided by two PZT-4 cylindrical transducers epoxied on the sides as shown. These transducers are 2.53cm long with an i.d. of 1.91cm, an o.d. of 2.54cm and a resonance frequency of about 50 kHz. Also epoxied to the cell are a minature PZT-5 pill transducer (to monitor the sound field) and an Omega Engineering model 44018 linear thermistor. The glass inlet and outlet tubes have an o.d. of roughly 3.5mm and are held in place by a

two hole rubber stopper. The inlet tube extends down to the mouth of the sphere in order to facilitate adaquate mixing when circulating the water. The entire sphere assembly is cradled in a monofilament line harness suspended from a square wooden frame which in turn is suspended from the top of a wooden box (Figure XII). The frame greatly simplifies the removal and replacement of the cell assembly and reduces the chance of accidentally dropping the sphere or knocking off a transducer.

Immediately below the resonator facing the flat is an RCA 6342A photomultiplier tube connected to an Ortec model 266 PMT base. Shielding is provided by a combination of a Mu metal jacket and grounded aluminum foil wrapping. The entire cell/PMT assembly is housed in a light tight box (Figure XIII) made of 1.8cm plywood with interior dimensions 59.7cm x 50.7cm x 58.1cm (HxWxD).

Due to the presence of the neck and the flat as well as all the mass loading, the resonant modes of the cell are extremely complex. We require a roughly spherical mode with a pressure antinode at the center. It is possible to suspend small gas-filled bubbles in an acoustic standing wave field where the buoyant force is balanced by a downward acoustic pressure gradient force. Subsequently, the introduction of gassy water makes it easy to observe the nature of the various modes and it was found empirically that the best mode, both in terms of spatial configuration and Q, occurs at a frequency of 61.725 kHz. Figure XIV is the result of a rudimentary field survey obtained by measuring the

spatial variation of the sound pressure amlitude along the axis of the sphere passing through the neck. This plot gives a rough estimate of the cell's "sensitive region": the volume of water where a cavitation event is most likely to occur. This volume is roughly

$$V_s \sim (4/3)\pi D^3 \quad , \tag{28}$$

where D is the half-width-at-half-max linear dimension of the principal peak. From the results of Figure XIV, $V_s \sim 1.8 cm^3$ when $P_a = 0.75$ Bar. Repeated observations with degassed water show that transient cavities do evolve in this region and nowhere else.

3.2 The Fluid Management System

Our goal was to design a system that allowed us to precisely monitor and control various liquid parameters such as surface tension, temperature, gas content, and nuclei size. Figure XV, which is fairly self explanatory, serves to illustrate our scheme (see also Figures XVI and XVII).

3.2.1 Materials Used

The most important aspect of the system is cleanliness, thus the choice of materials used is critical. Although the object of this particular study is water, we plan to perform similar measurements with alcohols

and various organic solvents. With this in mind, we chose teflon as the primary fluid handling material. All the fluid flow tubes are teflon TFE with an i.d. of 4.4mm and an o.d. of 6mm. The fluid flow valves (V5 through V8) are teflon TFE plug valves. A Micropump variable speed magnetic drive gear pump moves the liquid in a steady (non-pulsing) flow. The pump's fluid handling parts are all stainless steel, teflon and graphite. The in-line fluid filters are Teflon TFE 50mm diameter filters housed in a Teflon PFA filter holder. The "triple loops", which are securely wrapped in black electrical tape, provide a tortuous path for outside light which helps to preserve the integrity of the light tight enclosure. The reservoir, which holds about 2 liters, is made of glass and all the gas flow and evacuating pipes are aluminum.

3.2.2 Temperature Control

Temperature control and stability is provided via a Poly Temp model 90 constant temperature bath. This device circulates a water/antifreeze mixture through Tygon tubing first to a cooling jacket (a helical wrap of tubing) surrounding the reservoir and then to a 3 liter glass reservoir located inside the light tight box. The temperature monitoring circuit, which is drawn in Figure XVIII, features a switch that permits one to monitor alternatively the output of one of two matched thermistors mounted on the cell and the reservoir. The sensing circuitry (our design), which is composed of an operational amplifier

bridge circuit followed by a variable gain voltage amplifier, drives a Hewlett Packard model 3466A DMM which displays the temperature directly in millivolts (10mV/^{0}C). This system enables us to set repeatedly the cell temperature to 23.0±.5^{0}C from one run to the next despite wide variations in room temperature.

3.2.3 Surface Tension Measurement

Water samples used for these measurements are drawn from the system via valve V7. Surface tension determinations are made with a CENCO DuNOUY model 70535 tensiometer (see Figure XIX) which is essentially a mechanical balance that measures the force required to pull a platinum ring free from the surface of a liquid. This device gives consistent readings within an accuracy of a fraction of a percent.

3.2.4 *Control of Gas Concentration*

We "argonate" the water to a specified equilibrium gas pressure by simultaneously bubbling argon into the reservior, evacuating the reservoir and circulating the fluid. The rate of bubbling vis-a-vis the rate of evacuation (controlled respectively by valves V2 and V4) determines the reservoir pressure and thereby the gas pressure. The amount of time needed to reach equilibrium is estimated by performing repeated total gas content measurements with a volumetric Van Slyke

Apparatus [34] (see Figure XX), with the result that for a reservoir pressure of 0.5 Bar, equilibrium is attained in about 30 minutes. Note that the inlet from the argon bottle includes a 1μ in-line air filter, thus reducing the risk of contamination from dirty argon.

3.2.5 Control of Nuclei Size

Nuclei size control is achieved via extensive filtration; the filter size thus determines, in a sense, the nuclei size. Implicit in this statement is the assumption that the filter remains relatively clean. During the filtration process, the filters are replaced frequently and visual inspections reveal little or no observable deposits on the surface. The measured fluid flow rates during the filtrations are about 1 liter per minute. Since the total quantity of water in the system is about 2 liters, one can reasonably assume that the entire bulk of the fluid will will have made a pass through the filter in 5 minutes. Prior to each run, the sample undergoes simultaneous filtration and argonation for 45 minutes through filters that remain as clean as possible. We therefore assume that the nuclei size distribution has an upper bound that is approximately equal to, or slightly less than, the filter pore size.

3.3 The System Electronics

This discussion of the system electronics (Figure XXI) is divided into two parts:

(i) The acoustical power and frequency control system,

(ii) The gating, triggering and timing system.

To facilitate understanding, only simplified block diagrams are presented. We do not include components such as level matching amplifiers and signal terminators.

3.3.1 The Accustical Power and Frequency Control System

Figure XXII provides a block diagram of the circuitry that powers the cell. The heart of the system is a ramp generator (our design) that drives both the amplitude modulation input of a Hewlett Packard model 3312A function generator and a Fisher Series 5000 strip chart recorder. The DC voltage level of the strip chart record is linearly related to the peak to peak output amplitude of the function generator. This signal passes through an Arenberg attenuator, is amplified by an ENI model 1140LA power amp, which in turn drives the cell. Upon calibration, one determines the acoustic pressure amplitude in the cell simply by reading the strip chart record.

The signal generated by the pill transducer drives the vertical input of a Tektronix 7623 storage oscilloscope as well as the input of a digital resonance tracking circuit (our design). This device maximizes the RMS output of the cell by adjusting the frequency of the function generator (via the VCO input) to lay on resonance. A Hewlett Packard model 5314A universal counter monitors the frequency.

Since the acoustic pressure amplitude is essentially determined by the DC modulation signal, a "shutting down" of the sound field is tantamount to resetting the ramp generator to its quiescent "no ramp" state. The ramp generator exercises total control over the sound field while the strip chart recorder keeps a running record, in hard copy, of the pressure amplitude in the cell.

3.3.2 The Gating, Triggering and Timing Circuitry

Figure XXIII illustrates the electronics that generate the trigger pulses and provide timing control. The anode pulse from the photomultiplier tube base, upon amplification by three stages of an Ortec model 574 preamplifier, feeds into an Ortec model 473A pulse height discriminator. The discriminator level, which determines the sensitivity of the apparatus, is set to 600 mV, a value that is well above the electrical background level (~150 mV) but which lies below the typical sonoluminescence pulse height (~1.0 V). If the anode pulse

survives discrimination, it then passes through a "noise gating" network (described below) followed by a linear gate and finally results in the "trigger" pulse that subsequently resets the system. A "system reset" refers to a reduction in the sound pressure amplitude to a minimal quiescent level for a predetermined length of time. An Ortec model 776 timer provides the necessary control signals.

As an example of how the system works in a typical run, consider the system to be in its quiescent state where the sound field is off and the 776 is counting away. The timer disables both the linear gate and the ramp generator via the "busy" output, which is active whenever the 776 is counting. At the end of the timing sequence, the busy signal goes low which opens the linear gate and engages the ramp generator. The ramp proceeds until a transient event generates a pair of light pulses which, provided they survive amplitude discrimination and "noise" gating (more on this below), resets the timer and the whole process starts over. The linear gate prevents any stray noise pulses from resetting the timer before the quiescent period is over. In the event that a transient collapse does not generate a sufficient quantity of light to trigger the reset, the operator, who is monitoring the situation with headphones, can manually reset the system simply by pressing a botton.

Sonoluminescence is not the only source of light one encounters in this experiment. It turns out that a background "light noise" level of about 5 pulses per minute exists, probably due to Cerenkov radiation.

We desire a slow ramp rate; however, with stray noise signals occurring every 12 seconds or so, one cannot wait too long for cavitation to occur. Pulse height discrimination proves only partially effective since the brightest noise pulses are more intense than the weakest sonoluminescence events. We observe that, in this system, transient collapses almost always occur in bunches, some of the more catastrophic events generating hundreds of pulses in a matter of milliseconds. This fact inspired a "noise gating" scheme, diagrammed in Figure XXV, where the criteria for the generation of a trigger pulse is the occurence of two discriminator pulses separated by no more than 100 ms. The 473A has two outputs, one of which is connected directly to the "B" input of a Lecroy model 465 coincidence unit. The other undergoes a 20 ns delay (via a Tennelec model TC410A gate and delay module) and then activates the trigger of a BNC model 8010 pulser. This device produces a 100 ms gate signal that drives the "A" input of the coincidence unit. The time delay insures that the discriminator pulse, which is about 15 ns in width, reaches the coincidence unit before the gate signal. Thus, to establish coincidence, a second discriminator pulse must follow within 100 ms. The output of the 465 generates the trigger signal that resets the system. This technique allows us to halve the discriminator level while increasing the noise immunity by a factor of seven.

3.4 System Calibration

System calibration boils down to determining the acoustic pressure amplitude in the cell as a function of the strip chart voltage. We measure the pressure amplitude with a calibrated probe hydrophone composed of a PZT-5 cylinder roughly 1.6 mm long with an o.d. of about 1.6 mm mounted on the end of a long, thin rod. By monitoring the field at the secondary maxima (see Figure XIV), one avoids cavitation at the probe tip; however, this procedure requires knowledge of the relationship between the acoustic pressures at the secondary and primary maxima over the range of amplitudes encountered in this experiment. Figure XXVI is a plot of the primary pressure, P_p, versus the secondary pressure, P_s, over the range of amplitudes for which cavitation does not occur, which is severely limited due to the presence of the probe at the primary maxima. This measured relationship, which is clearly linear, is assumed to hold true for the entire range of pressure amplitudes encountered.

The next step involves choosing a "reference configuration" of equipment settings used to calibrate the system. Reproducing this configuration prior to each data run ensures that the system is properly calibrated for that particular experiment. Initializing the system to its reference configuration is a three step process.

A: The ramp generator (modulation) voltage is set to -2.250 V and the gain of the function generator adjusted so that the output of the pill is 50 mV_{p-p} with the Arenberg attenuator set to -20dB.

B: The modulation voltage is lowered to -2.400 V and the pen of the strip chart recorder adjusted to read 0.0 V.

C: The modulation voltage is further reduced to -2.600 V. At this point the acoustic pressure amplitude in the cell is essentially zero. This is considered to be the system's "quiescent state".

One should be aware that with the exception of the quiescent ramp voltage, our choice of the above parameters is motivated primarily by convenience.

With the system suitably initialized, the acoustic pressure in the cell is now ramped while the RMS voltage output from the probe is monitored. Some typical results are presented in Figure XXVII. The solid line is a computer fit to the data points, each of which is a arithmetic mean of 5 measurements. The resulting system calibration is given by

$$P_a = 2.87V_s + .91 \quad , \tag{29}$$

where V_s is the strip chart voltage and P_a is the acoustic pressure amplitude (in Bars) at the primary maximum of the sphere.

Chapter 4

EXPERIMENTAL PROCEDURE

4.1 Sample Preparation

The water samples used in this investigation are triply distilled and deionized. Upon introduction of the water into the reservoir, the fluid flow system is disturbed only in order to change the filter or to draw a 10 ml sample used for surface tension and gas content measurements. All the data are taken with the same water at the same temperature, surface tension and gas content. Repeated surface tension determinations yield the value 71.3 dynes/cm with great regularity. Using the system described in section 3.3.2 we set the cell temperature to 23.0±.5°C, a value that increases by roughly 0.5°C over the course of a two hour experiment. The control of nuclei size and gas concentration is a four step process.

A: The water sample is introduced and filtered down to the desired nuclei size, with extreme care being taken not to let the filters get dirty. Initially we replace our filters every few minutes and the whole process takes the better part of a day.

B: A fresh filter is installed and the liquid is circulated for 45 minutes while simultaniously bubbling argon through the water and evacuating the reservoir. Using valves V1 and V2 the reservoir pressure is set to 0.5 Bar, thus insuring an equilibrium gas pressure of 0.5 Bar.

C: The circulation pump is turned off and the reservoir pressure is gradually restored to atmospheric.

A: The cell is allowed to stand undisturbed for one hour before beginning to take data. This waiting period allows for the dissolution of any non-stabilized microbubbles in the resonator.

We repeat steps (B) through (D) prior to every data run, whereas step (A) follows every change of filter size.

4.2 Data Acquisition

The process of data acquisition begins with the system set to its reference configuration. This procedure is described in section 3.4. Recall that we desire a time interval between measurements during which the system is in its "quiescent state" (when the sound field is off and the ramp is disabled). The need for this dormant period stems from the fact that, when a bubble (or a group of bubbles) undergoes a violent collapse the collapsing bubble "seeds" the water with smaller, nonstabilized microbubbles. The extent of the seeding may or may not be significant. However, to be safe we allow 300 seconds for dissolution

to take place. Empirical observatations indicate that a significant reduction in this quiescent time does not affect the mean experimental threshold; the standard deviation, however, does increase. Upon setting the 776 to count off a 300 second interval, one presses the timer's reset button and the following process begins.

A: The 776 timer counts to 300, one second at a time. This marks the end of the quiescent interval.

B: The timer engages the ramp generator and the optical triggering circuitry. The acoustic pressure amplitude in the cell increases at a rate of about 0.2 Bar per second.

C: Upon reaching the threshold pressure a transient event takes place, resulting in an audible (via the headphones) "click" and, in most cases, a sonoluminescent flash.

D: If light emission occurs, the system automatically resets to its quiescent state. Otherwise, the operator manually disengages the apparatus by pressing a reset button.

E: The above sequence of events repeats itself as long as the operator wishes.

Figure XXVIII is a reproduction of the chart record for a typical data run. Each run consists of 15 data points. We establish reproducibility by repeating the experiment twice for each filter size. Thus, each experimentally determined threshold value is the arithmetic mean of 30 individual measurements taken on two different occasions. Table II provides a restatement of the basic experimental parameters.

Sample	triply distilled and deionized water
Temperature	23°C
Surface Tension	71.3 Dynes/cm
Equilibrium Gas Pressure	0.5 Bar
Nuclei Size	4 filter pore sizes; 20μ, 10μ, 5μ and 1μ
Discriminator	600 mV
Coincidence Requirement	2 pulses within 100 ms
Quiescent Acoustic Pressure Amplitude	~0.1 Bar
Quiescent Time Period	300 seconds
Ramp Rate	0.2 Bar/sec
Frequency	61.725 kHz

TABLE II EXPERIMENTAL PARAMETERS

Chapter 5

RESULTS AND CONCLUSIONS

5.1 Experimental Results

The purpose of this investigation is to measure transient cavitation thresholds in water as a function of nuclei size, which we control via protracted filtration. Table III summarizes the results of these measurements. The first column gives the approximate nuclei diameter based on the filter employed. The second column records the experimentally measured threshold values, along with the standard deviations for each individual data run. The third column in Table III presents what we call the "sonoluminescence occurence ratio" (SOR) which is the percentage of data points in a given run that result in light emmision. The SOR provides an indication of the effectiveness of using sonoluminescence in predicting the same cavitation threshold that one obtains when listening for an audible shock wave.

The results in Table III are plotted in Figure XXIX, which is a graph of transient cavitation threshold versus nuclei size. The error bars correspond to the computed standard deviations. Also plotted are the predicted free bubble thresholds (eq. (18)) and the crevice model

threshold (eq. (26)). Neither theory provides a particularly good fit to experimental data. Note that the crevice model exhibits quantitative agreement at large filter sizes but fails to explain the increase in threshold for smaller nuclei. The free bubble model predicts a rise in threshold at small R_o; however, there is poor quantitative agreement between theory and experiment at all nuclei sizes. The possible reasons for these many discrepencies are the subject of the paragraphs that follow.

NUCLEI SIZE (μ)	THRESHOLD (Bars)	SOR
20	4.36±.26	.93
	4.12±.26	.93
10	5.33±.44	.80
	5.23±.35	.87
5	7.21±.71	.33
	8.06±.70	.66
1	7.75±.91	.53
	7.62±.84	.53

Summary of Results

NUCLEI SIZE (μ)	THRESHOLD (Bars)	DEVIATION	SOR
20	4.24±.29	6.9%	.93
10	5.30±.40	7.6%	.84
5	7.63±.84	11.0%	.70
1	7.69±.89	11.6%	.53

TABLE III EXPERIMENTAL RESULTS

5.2 Relationship Between Theory and Experiment

5.2.1 Free Bubble Model

The first question to be asked is what exactly does filtration do to influence the size distribution of stabilized microbubbles. Ionic skins should simply break up, pass through the filter, and reform on the other side. Thus, if ions are the primary stabilization mechanism, there should be little change in measured thresholds even when filtering down to 0.1μ. We have attempted to measure the threshold of extensively filtered water and found that it exceeded the capabilities of our resonator, which can generate a maximum acoustic pressure amplitude of about 15 Bars. This result, which is consistent with the measurements of Greenspan (see section 1.1.1.2), leads us to conclude that ions do not play a major role in stabilizing microbubbles in our water.

Yount maintains that his organic skins are tough enough to survive filtration [35]; however, one must keep in mind the fact that a nucleus which stabilizes to some radius at some ambient pressure will stabilize at a smaller radius if the ambient pressure is increased. Recall that after "Argonation" at a pressure of 0.5 Bar, the sample stands for one hour at atmospheric pressure. It is therefore conceivable that the upper bound placed on the nuclei distribution is significantly less than the filter pore size. This may help to explain why the measured

thresholds begin to increase at larger filter sizes than the free bubble theory predicts, but does nothing to reconcile the difference in quantitative results.

It may be overly simplistic to assume that, aside from establishing the equilibrium radius, the stabilization mechanism plays no role in determining the transient cavitation threshold. In Apfel's treatise on acoustic cavitation prediction [22], he introduces the concept of a startup time: the minimum time before significant growth can get started. Although the influence of an organic skin is most likely minimal just before a cavity becomes transient, it is possible that the skin might retard the initial growth. If the startup time assocated with "skin resistance" is a significant fraction of the available growth time ΔT (see eq. 17), then the theory must be modified to include the role of the skin. Such a modification would likely result in an increase in the predicted thresholds.

Finally, one must consider the applicability of the growth equation (eq. 13) itself. Neppiras [23] views this result as an approximate expression which applies only to large bubbles (where surface tension is not very influential). Apfel himself asserts that the theory is "not really valid" for predicted threshold pressures of less than 2 Bars, which happens to be our range of operation. An outstanding feature of the free bubble theory is that it predicts transient cavitation thresholds that are proportional to $R_o^{6/5}$. Unfortunately, this

experiment is not sensitive to such behavior for implicit in its design is the assumption that the larger nuclei have a lower threshold and therefore cavitate first. A more meaningful, and considerably more difficult, approach would be to establish both a lower and upper bound to the nuclei size distributions. Thus, the system would be sensitive to thresholds that either increase or decrease with decreasing nuclei size.

5.2.2 Crevice Model Thresholds

When studying cavitation phenomena, it is of utmost importance that the investigator know as much as possible about the physical properties of the fluid under study. In this experiment, we can adequately control various bulk liquid parameters such as temperature, surface tension and gas content, but the only thing we know about the nuclei is the approximate upper bound to their size distribution. The crevice model is inextricably tied to the specific surface characteristics and crack geometry of the motes in our water. Note that the data that Crum used in determing the parameters δ and θ (see eq. 26) were taken with nonfiltered water. This fact is consistent with the observed agreement between his theory and our results for larger filter sizes. However, to generalize these parameters to motes as small as 1μ may be too restrictive. We must consider the possibility that the geometrical characteristics of the crevices may be different. Also the small dirt

particles may be of a totally different nature (chemically) than large particles. The crevice model correctly predicts transient cavitation thresholds for large (>10μ radius) motes

however, without further information concerning the nature of our dirt, meaningful analysis of the small particle data vis-a-vis the crevice model proves difficult.

5.3 Experimental Uncertainties

There are numerous sources of error in this experiment, both statistical and systematic. We list some of them below.

SOURCE OF ERROR	ESTIMATED UNCERTAINTY
Surface Tension Measurement	<0.5%
Temperature Control	~2.0%
Gas Content Control	~2.0%
Frequency Control	<.05%
Strip Chart Record	~1.0%
Human Reaction Time	<2.0%
Uncertainty in System Initialization	<2.0%

TABLE IV EXPERIMENTAL UNCERTAINTIES

With the exception of human reaction time, all the above errors are statistical in nature and will not significant influence the measured transient thresholds. There are, however, three sources of error that we feel will significantly affect our results.

(A) RAMPING ERROR: Filtering the water does more than just set an upper bound to the nuclei size distribution; it also reduces the total number of nuclei in the liquid. Thus, there is an increased probability that a low threshold nuclei will not be in the sensitive region when the threshold pressure is reached. Eventually, a transient event will take place, but a time delay of only a second corresponds to an error of 4%. This is our primary motivation for choosing as slow a ramp speed as the background noise allows (see section 3.3.2). The ramping error is both statistically and systematically significant, resulting in effectively higher measured thresholds and larger standard deviations as the filter size decreases.

(B) FILTERING ERROR: Despite all of our precautions, it is still likely that nuclei smaller than the filter size fail to survive a pass through the filter. Therefore, the upper bound to the nuclei size distribution is probably somewhat less than the filter pore size. This helps to explain why the measured thresholds begin to increase at larger filter sizes than the free bubble theory suggests. However the discrepency in quantitative results remains unresolved. Note that excessive filtration further depletes the nuclei available to cavitate, thus compounding the ramping error discussed above.

(C) CALIBRATION ERROR: Implicit in the calibration process is the assumption that the ratio of the primary to the secondary pressure maxima in the cell remains constant over the range of

acoustic pressure amplitudes encountered in this experiment. This assumption may be excessively restrictive. We observe while ramping that harmonics begin to occur at a pressure amplitude of about 7 Bars, a behavior which may be accompanied by a reduction in the Q of the resonator. Such behavior would tend to increase the measured cavitation thresholds. The only way to determine the precise nature of the sound field at all "working" amplitudes is to survey it with a hydrophone. The introduction of a probe at amplitudes greater than a few Bars generates instant cavitation activity at the probe tip, resulting in a damaged hydrophone and meaningless measurements. We see no clear cut resolution to this problem.

5.4 The Question of Sonoluminescence

We have yet to determine whether or not sonoluminescence is an effective threshold indicator. The fact that the SOR decreases with decreasing filter size suggests that, as nuclei sizes get smaller and smaller, the thresholds for sound emission and light emission diverge, the latter having the higher threshold. Neppiras [23] has shown that the temperature generated by a collapsing bubble is proportional to the maximum radius it grows to, which, at the threshold for sound emission ($R_m=2.3R_o$), decreases with decreasing nuclei size. Also, the amount of light emitted is proportional to the amount of gas available to react,

which is also reduced at smaller bubble (or mote) sizes. Thus, an increase in sonoluminescence threshold for smaller filter sizes comes as no surprise.

One may be tempted to ask which threshold is "correct". The answer is that they both correctly indicate the threshold for two different types of phenomena. Suppose one is interested in predicting the minimum acoustic threshold pressure necessary to initiate a violent reaction. Then the sonoluminescence threshold may prove to be the more significant parameter since the violence of a transient event is linked primarily to R_m, which corresponds to the energy stored in the liquid. Thus, sonoluminmescence may serve as an ideal indicator of what Apfel calls the "threshold for transient-violent cavitation" [22].

5.5 Instrument Improvement

In its present form, this apparatus is ideally suited to making fully automated sonoluminescence threshold measurements and operator assisted sound emission threshold measurements in a simple and reproducable manner. Measured transient cavitation thresholds show quantitative agreement with the results of Crum [18], Brosey [27], Strasberg [16], Barger [36] and others with a precision that, to our knowledge, is unprecedented in the literature. However, there are many ways in which one can improve the versatility and performance of the apparatus.

(1) Introducing in-line deionization and organic removal columns to improve control over the purity of the water.

(2) Improve the heat exchange characteristics of the cooling system, possibly by replacing the glass cooling resevoirs (in the box) with copper tubes. The present system proves effective, yet requires a considerable amount of operator management.

(3) Improve the performance of the resonator, making it easier to calibrate and capable of generating higher acoustic pressure amplitudes. One might consider trying a cylindrical geometry or a focused transducer, the latter being more appropriate for high frequency measurements.

(4) Introduce circuitry that can "listen" for the occurence of sound emission and automatically generate a system reset. Thus, one would be able to measure the threshold for sound emission in an automated fashion. With appropriate detection schemes, one could pursue this reasoning further and perform automated measurements of quantities such as the thresholds for subharmonic emission, neutron induced cavitation, rectified diffusion etc.

(5) Reduce the ramp rate or introduce a DC staircase generator. Such a device would hold the acoustic pressure at a constant value for a specified length of time and then automatically step up to the next desired pressure setting. This would greatly reduce the problems associated with "ramp error" but would increase the likelihood of a noise event falsely triggering the system (see page 34).

(6) Computerize the entire experiment. A digital computer can easily control the ramp or staircase, provide the system reset, record and store the threshold values, and even circulate and degass the liquid.

5.6 Concluding Remarks

In this study we have examined, both theoretically and experimentally, the relationship between cavitation nuclei size and transient cavitation thresholds. For large nuclei, experimental observations agree with crevice model predictions both qualitatively and quantitatively. For smaller nuclei (R_o less than about 5μ) the experimental and crevice model curves deviate significantly, the former exhibiting characteristics consistent with free bubble model predictions. There is poor quantitative agreement between experiment and free bubble theory for all nuclei sizes. Several factors which may be contributing to the observed deviations include:

(i) Insufficient information concerning the chemical and geometric nature of the motes in the water (especially for smaller motes).

(ii) The assumption that stabilization mechanisms do not affect free bubble dynamics.

(iii) The limited applicability of the free bubble theory in the region where predicted transient cavitation threshold pressures are less than 2 Bars.

(iv) Systematic experimental errors such as uncertainties in controlling the maximum nuclei size via filtration, system calibration error and ramping error.

We have developed an apparatus that performs threshold measurements in an automated and reproducable manner. Critical fluid parameters such as physical and chemical cleanliness, dissolved gas concentration, temperature, etc. are easily monitored and controlled. We have employed both sound emission and sonoluminescence as transient cavitation indicators and found that for larger nuclei the two techniques provide the same information whereas for smaller nuclei (R_o less than about 5μ) sonoluminescence thresholds appear higher. Since light emission is linked primarily to collapse temperatures and pressures, we postulate that sonoluminescence may be a good indicator of "transient-violent cavitation", an idea that warrants further investigation.

BIBLIOGRAPHY

[1] P.S. Epstein and M.S. Plesset, J. Chem. Phys. 18, 1505 (1950)

[2] F.E. Fox and K.F. Hertzfeld, J. Acoust. Soc. Amer. 26, 985 (1954)

[3] M. Strasberg, J. Acoust. Soc. Amer. 31, 163 (1959)

[4] D.E. Yount, T.D. Kunkle, J.S. D'Arrigo, F.W. Ingle, C.M. Yeung and E.L. Bechman, Av. Space and Envn. Med. 48, 185 (1977)

[5] D.E. Yount and C.M. Yeung, J. Acoust. Soc. Amer. 69, 702 (1981)

[6] D.E. Yount, J. Appl. Phys. 47, 5081 (1976)

[8] H.A. McTaggort, Phil. Mag. 27, 297 (1914)

[9] T. Alty, Proc. Roy. Soc., Ser. A 106, 315 (1924)

[10] T. Alty, Proc. Roy. Soc., Ser. A 112, 235 (1926)

[11] V.A. Akulichev, Sov. Phys. Acoust. 12, 144 (1966)

[12] M.G. Sirotyuk, Sov. Phys. Acoust. 16, 237 (1970)

[13] E.N. Harvey, D.K. Barnes, W.D. McElroy, A.H. Whiteley, D.C. Pease, and K.W. Cooper, J. Cell Comp. Physiol. 24, 1 (1944)

[14] M. Greenspan and C.E. Tschiegg, J. Res. Natl. Bur. Stand. C71, 299 (1967)

[15] R.H.S. Winterton, J. Phys. D.: Appl. Phys. 10, 2041 (1977)

[16] M. Strasberg, J. Acoust. Soc. Amer. 31, 163 (1959)

[17] R.E. Apfel, J. Acoust. Soc. Amer. 48, 1179 (1970)

[18] L.A. Crum, Nature 278, 148 (1979)

[19] D. Lieberman, Phys. Fluids 2, 466 (1959)

[20] L. Crum, Personal Communication, (1982)

[21] F.G. Blake, Jr., "The Onset of Cavitation in Liquids" Tech. Memo No. 12, Acoustics Research Lab, Harvard Univ. (1949)

[22] R.E. Apfel, J. Acoust. Soc. Amer. 69, 1624 (1981)

[23] E.A. Neppiras, "Acoustic Cavitation" in Physics Reports, Vol. 61. North-Holland, Amsterdam (1980)

[24] D. Bargeman and F. Van Voorst Vader, J. Coll. Sci. 42, 467 (1973)

[25] D. Bargeman, J. Coll. Sci. 40, 344 (1972)

[26] C.G.L. Furmidge, J. Coll. Sci. 17, 309 (1962)

[27] J. Brosey, "The Effect of Polymer Additives on the Cavitation Threshold of Water" Tech. Report No. 811, ONR (1982)

[28] P. Jarman, Proc. Phys. Soc. 73, 628 (1959)

[29] T.K. Saksena and W.L. Nyborg, J. Chem. Phys. 53, 1772 (1970)

[30] R.O. Prudhomme and T. Guilmart, J. Chem. Phys. 54, 336 (1957)

[31] M.G. Sirotyuk, Proc. 4th Int. Conf. Acoust. (Copenhagen, 1962), Pater 03U 26.

[32] R.D. Finch, Ultrasonics 1, 87 (1963)

[33] H.G. Flynn, "Physics of Acoustic Cavitation in Liquids" in Physical Acoustics (W.P. Mason, ed.) Vol. IB. Acad. Press, New York (1964)

[34] D.D. Van Slyke and W.C. Stadie, J. Bio. Chem. 49, 1 (1921)

[35] D.E. Yount and C.M. Yeung, J. Acoust. Soc. Amer. 65 (1979)

[36] J. Barger, J. Acoust. Soc. Amer. 31, 163 (1959)

APPENDIX

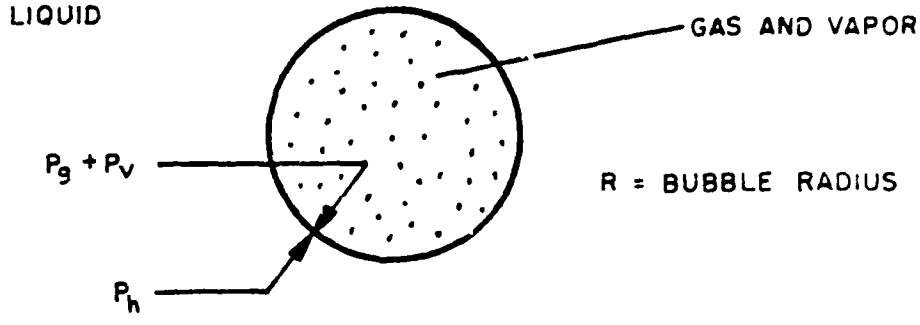

FIG. I FREE BUBBLE

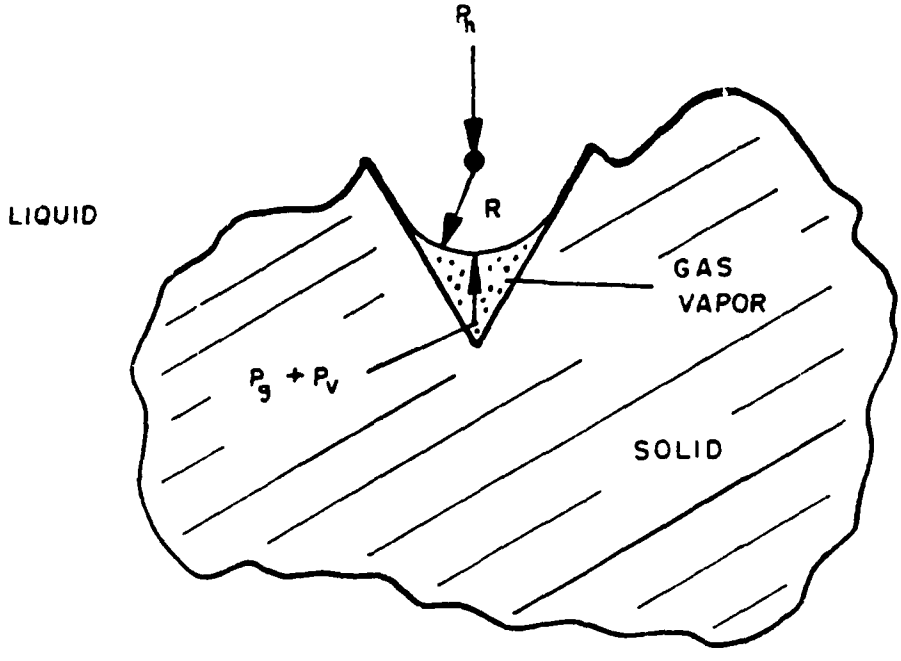

FIG. II GAS CAUGHT IN A CRACK

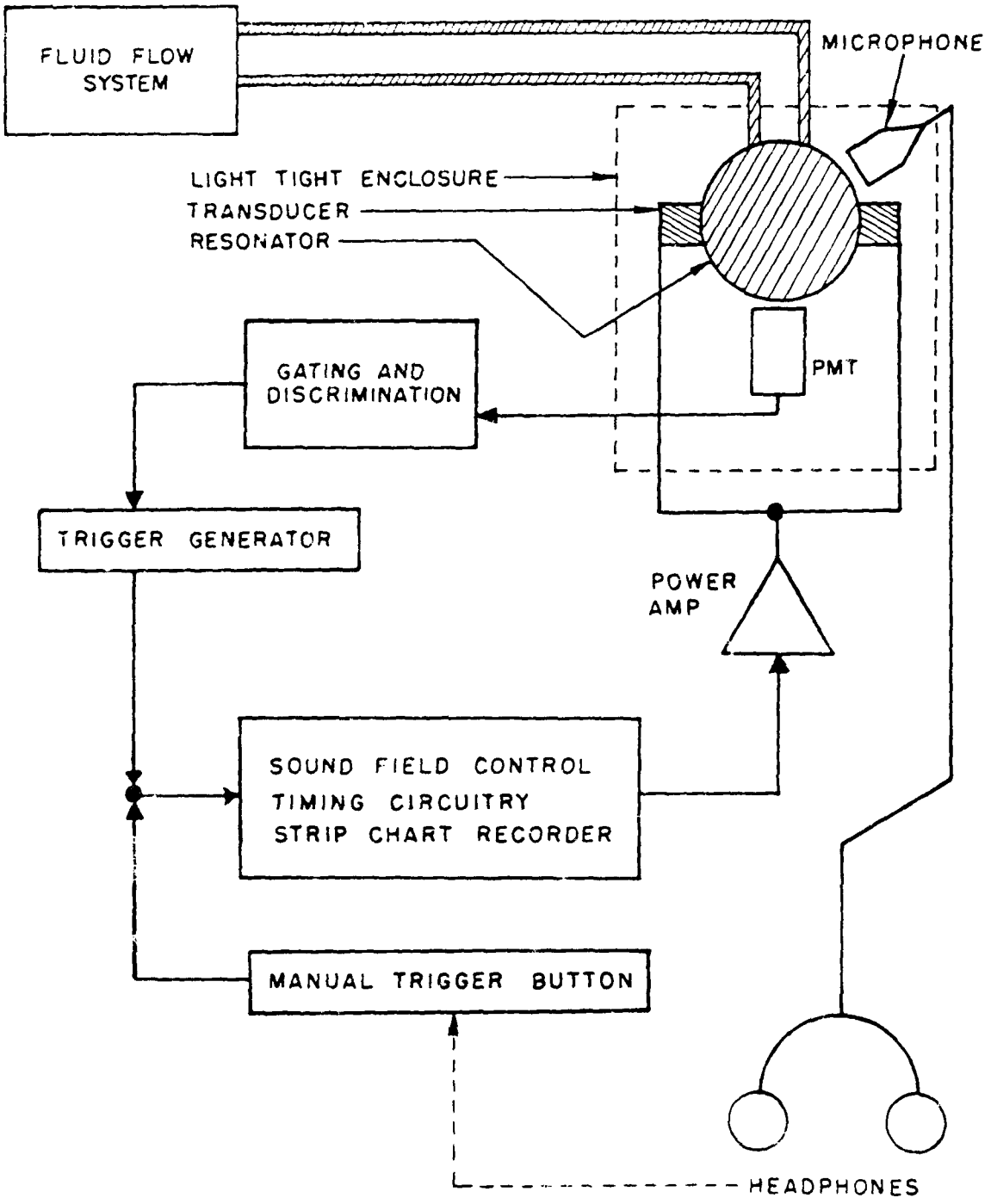

FIG. III SIMPLIFIED EXPERIMENTAL ARRANGEMENT

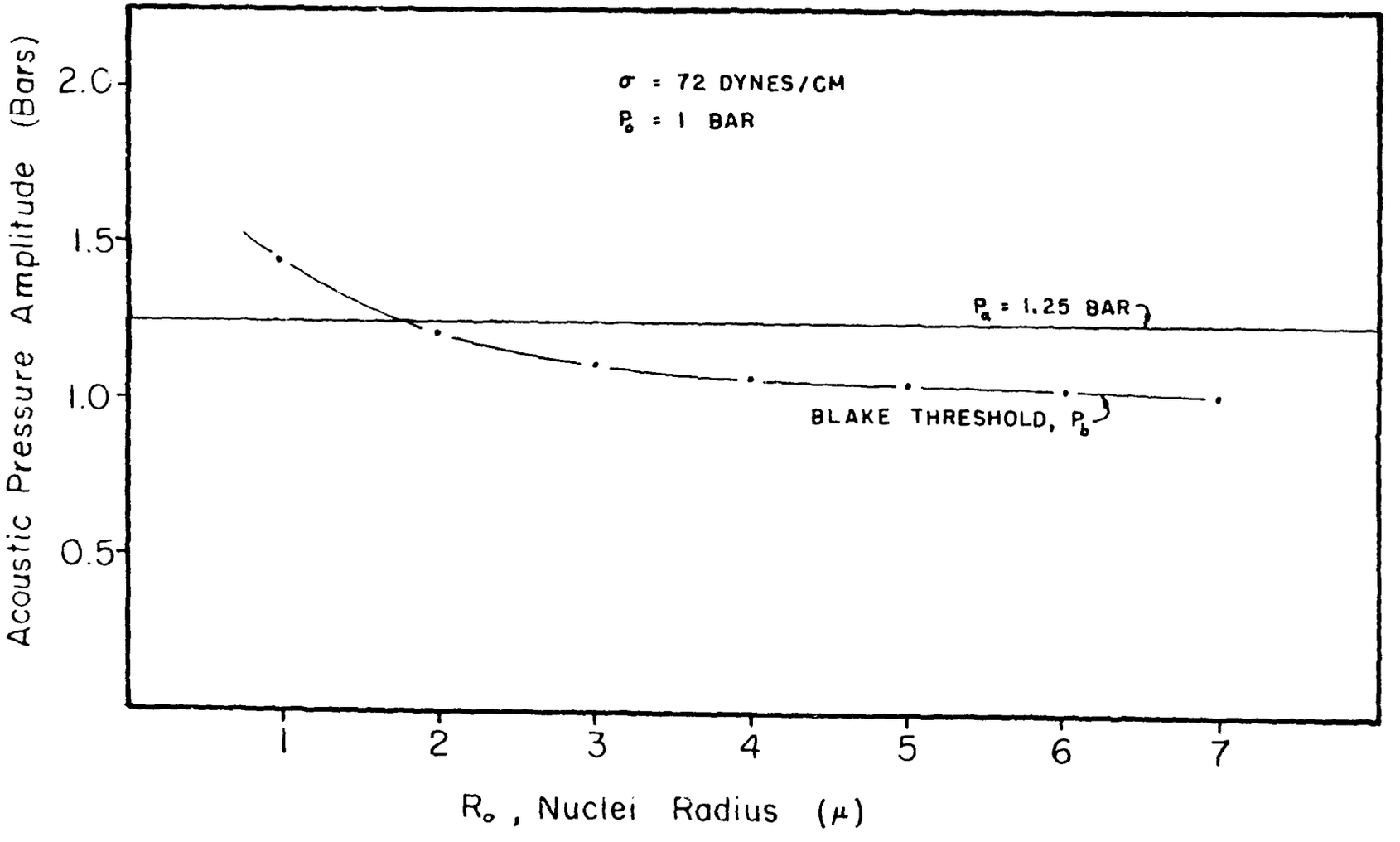

FIG. IV BLAKE THRESHOLDS

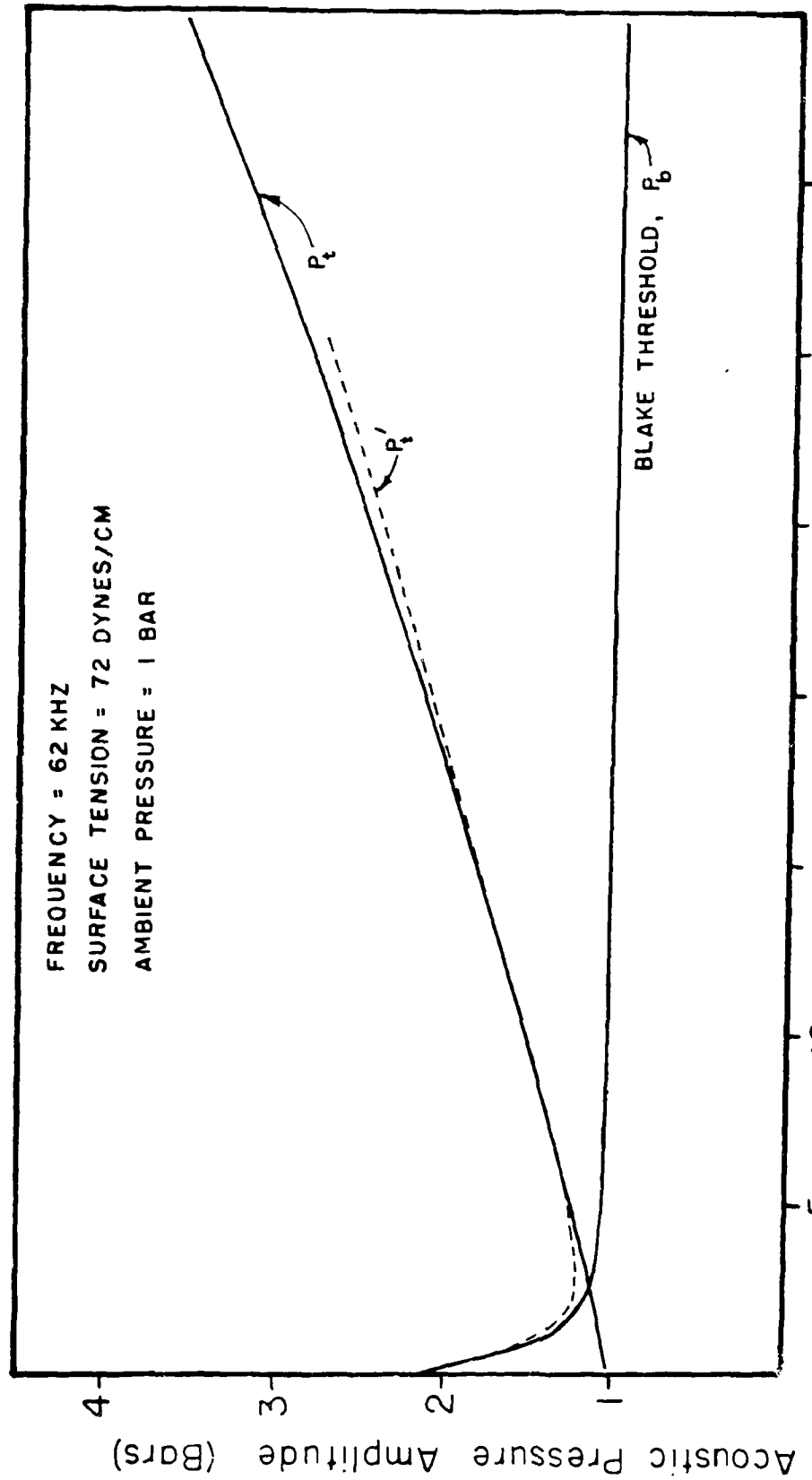

FIG. V FREE BUBBLE THRESHOLDS

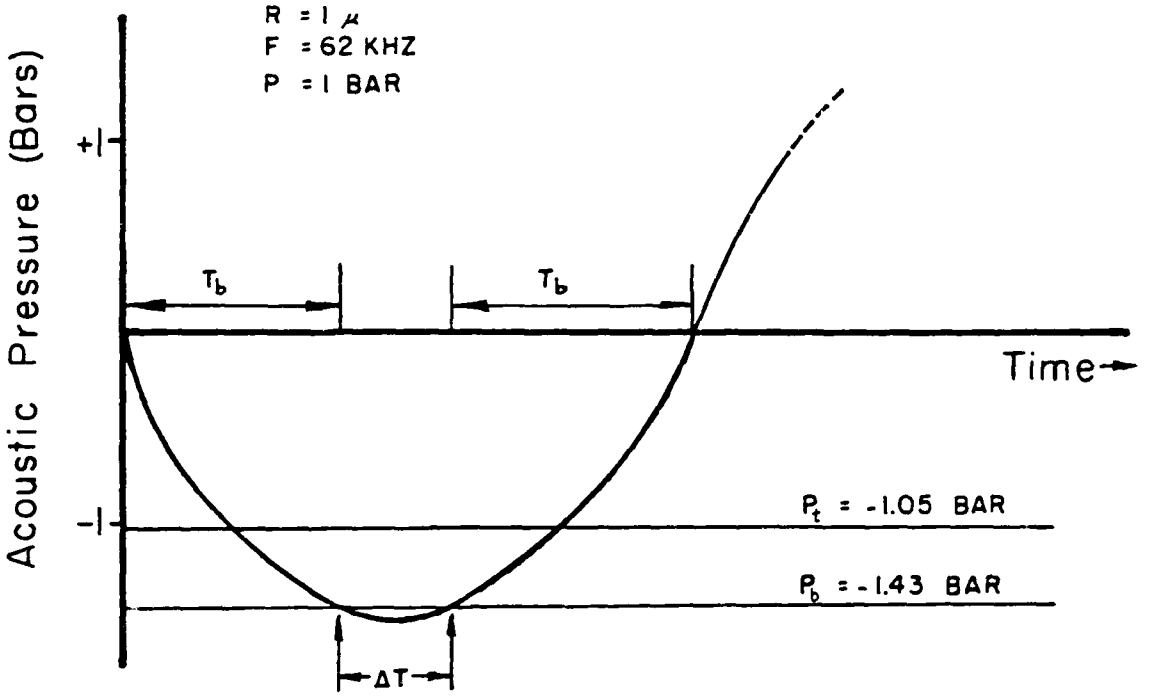

FIG. VI ILLUSTRATED GROWTH TIMES

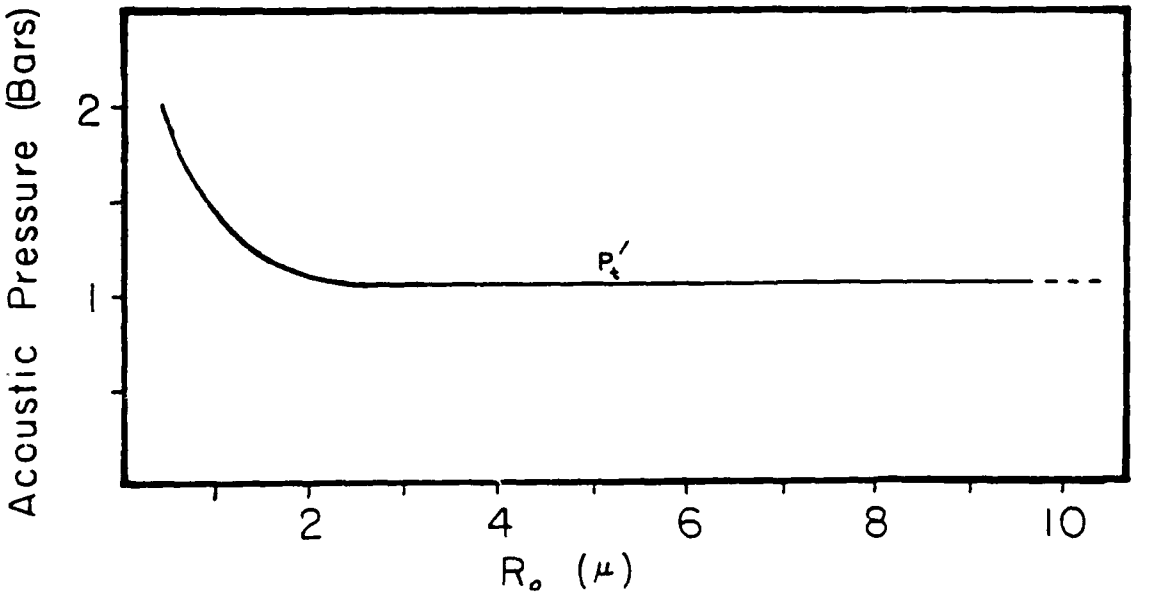

FIG. VII MODIFIED FREE BUBBLE THRESHOLDS

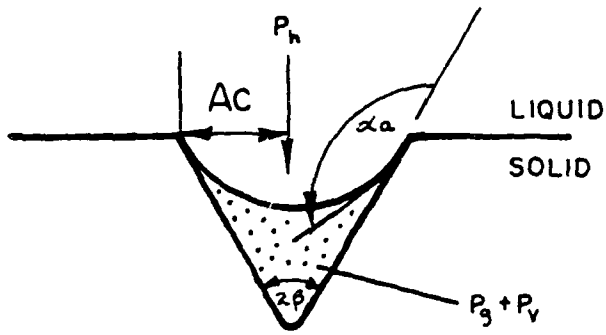

FIG. VIII CRITICAL CREVICE

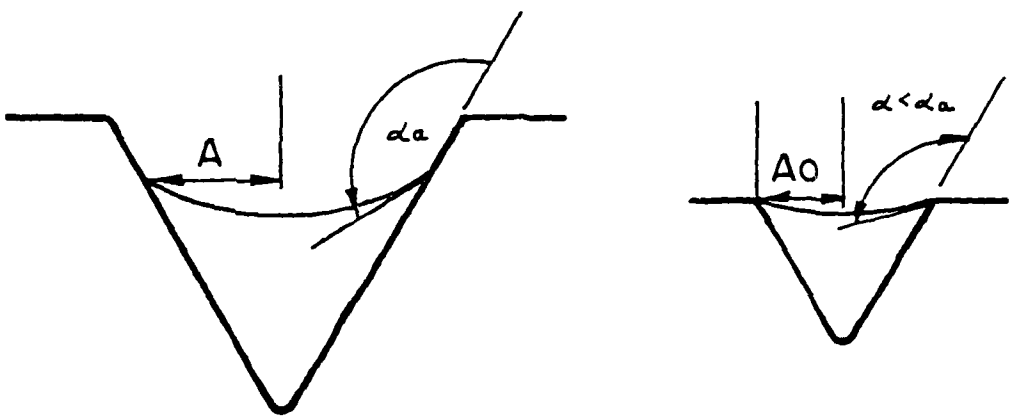

FIG. IX NONCRITICAL CREVICES

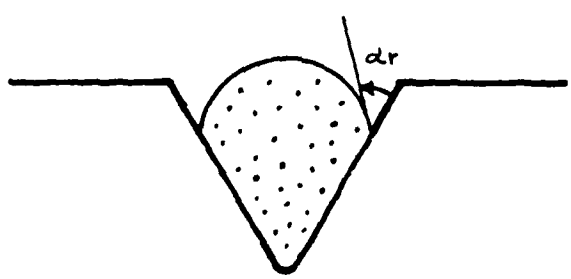

FIG. X NUCLEATING BUBBLE

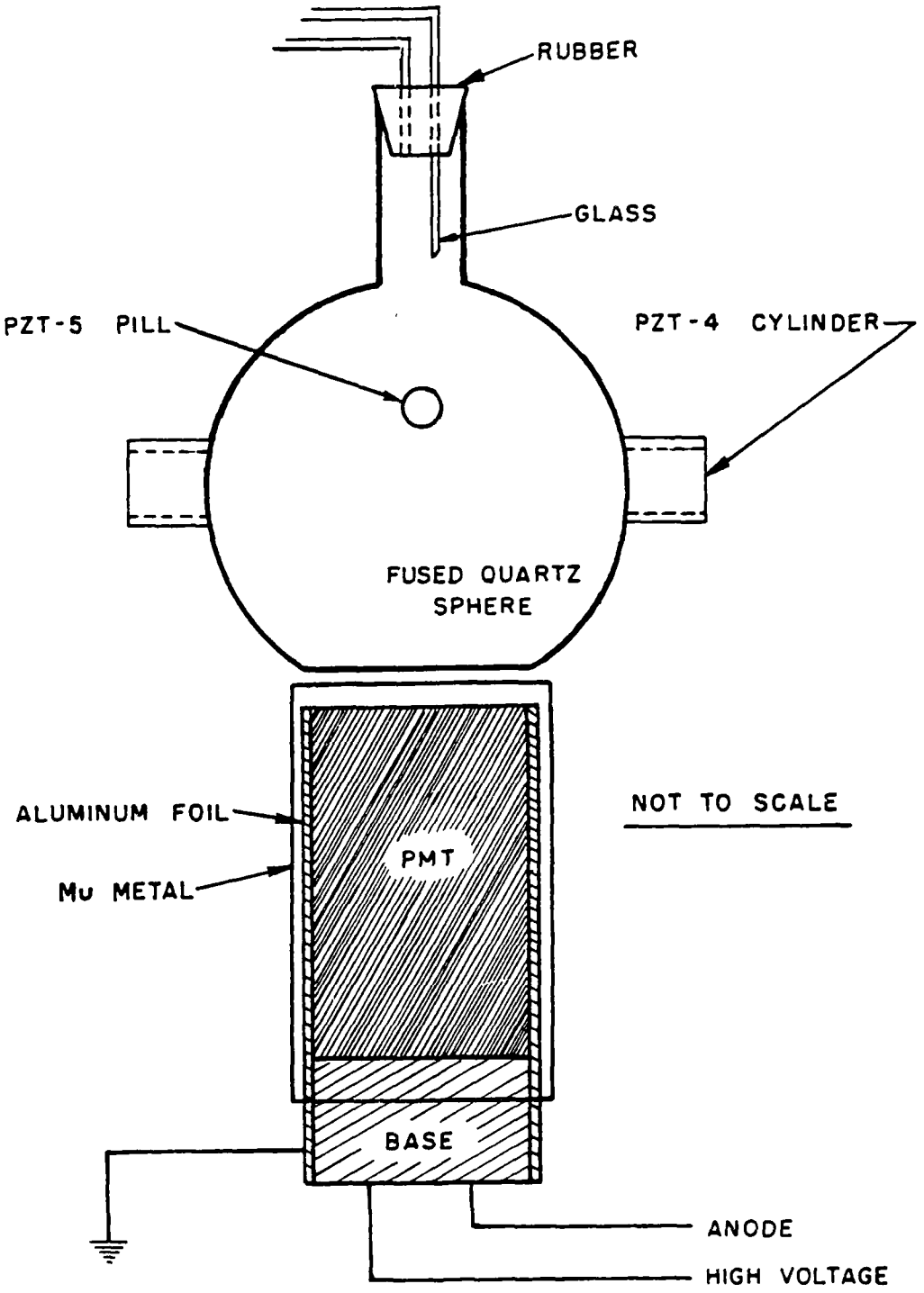

FIG. XI RESONATOR/PMT ASSEMBLY

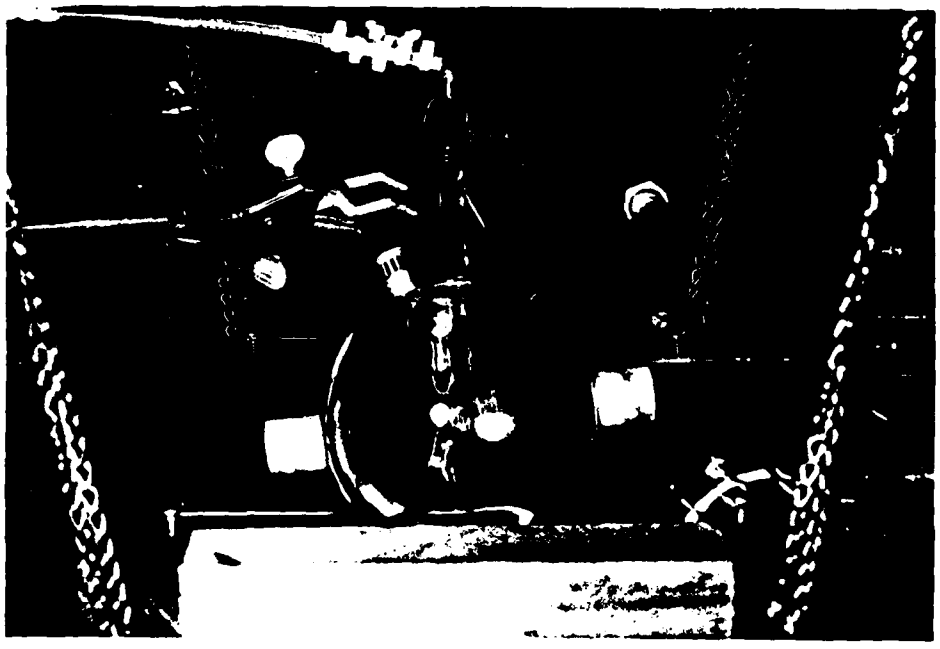

FIG. XII RESONANT SPHERE ASSEMBLY PHOTO

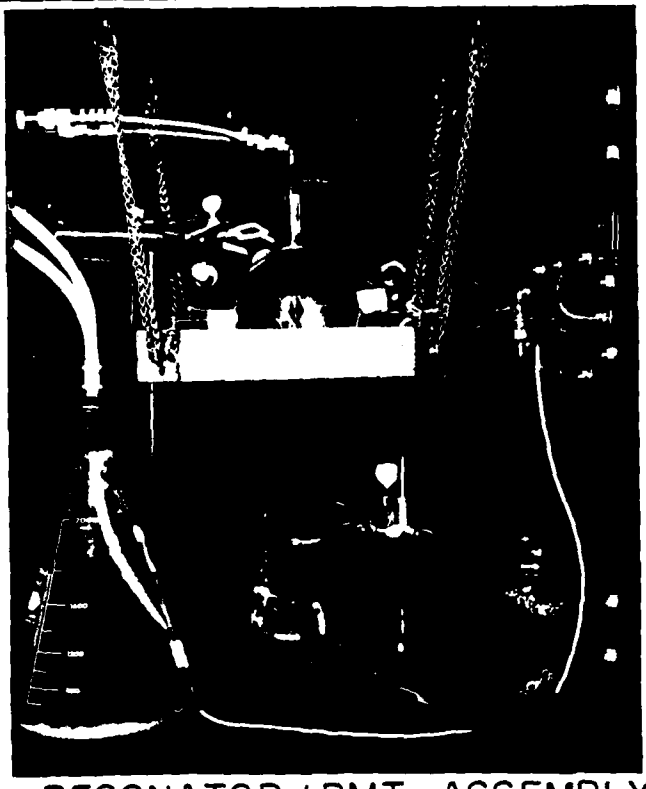

FIG. XIII RESONATOR/PMT ASSEMBLY PHOTO

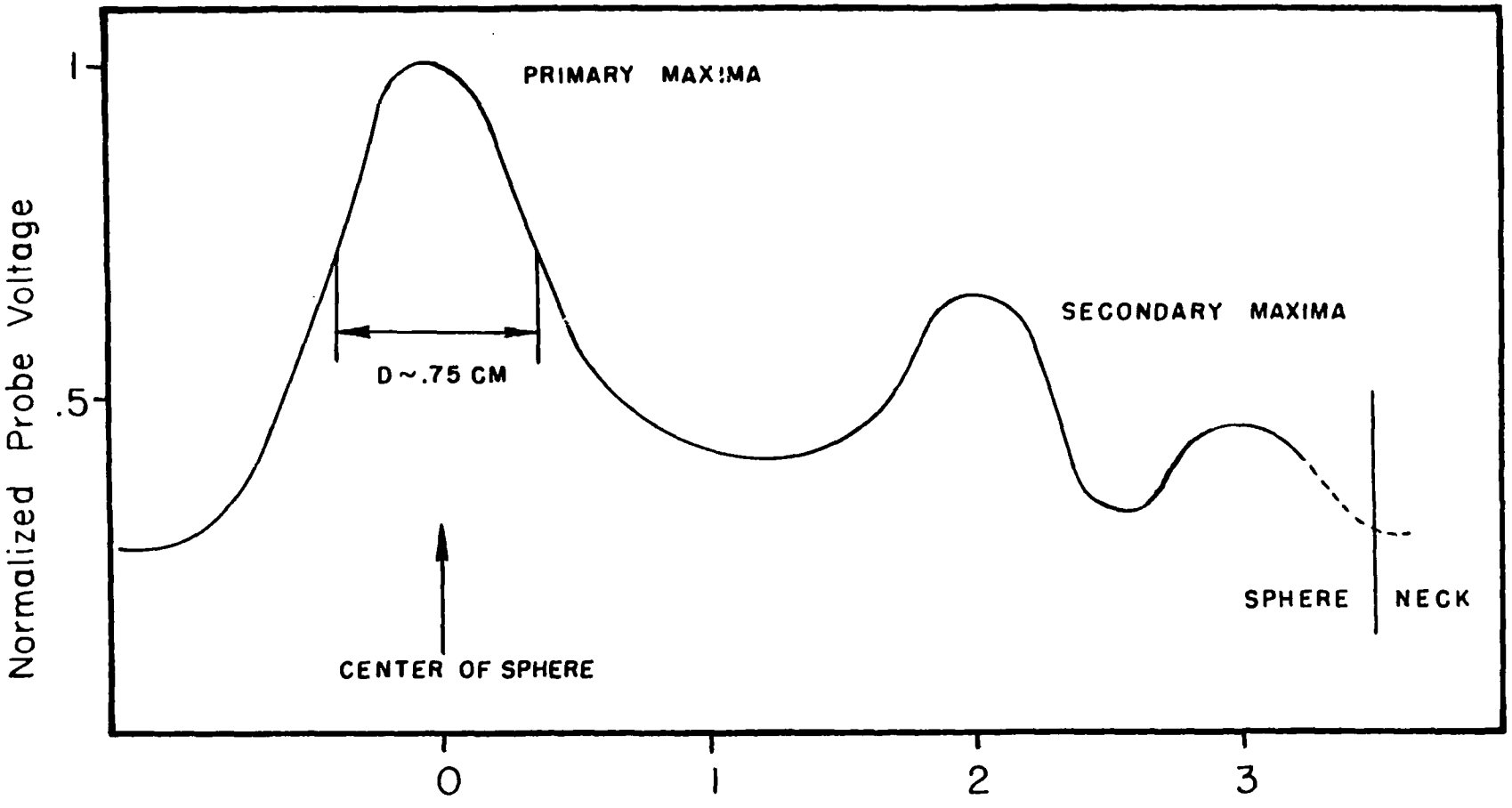

FIG. XIV AXIAL FIELD SURVEY

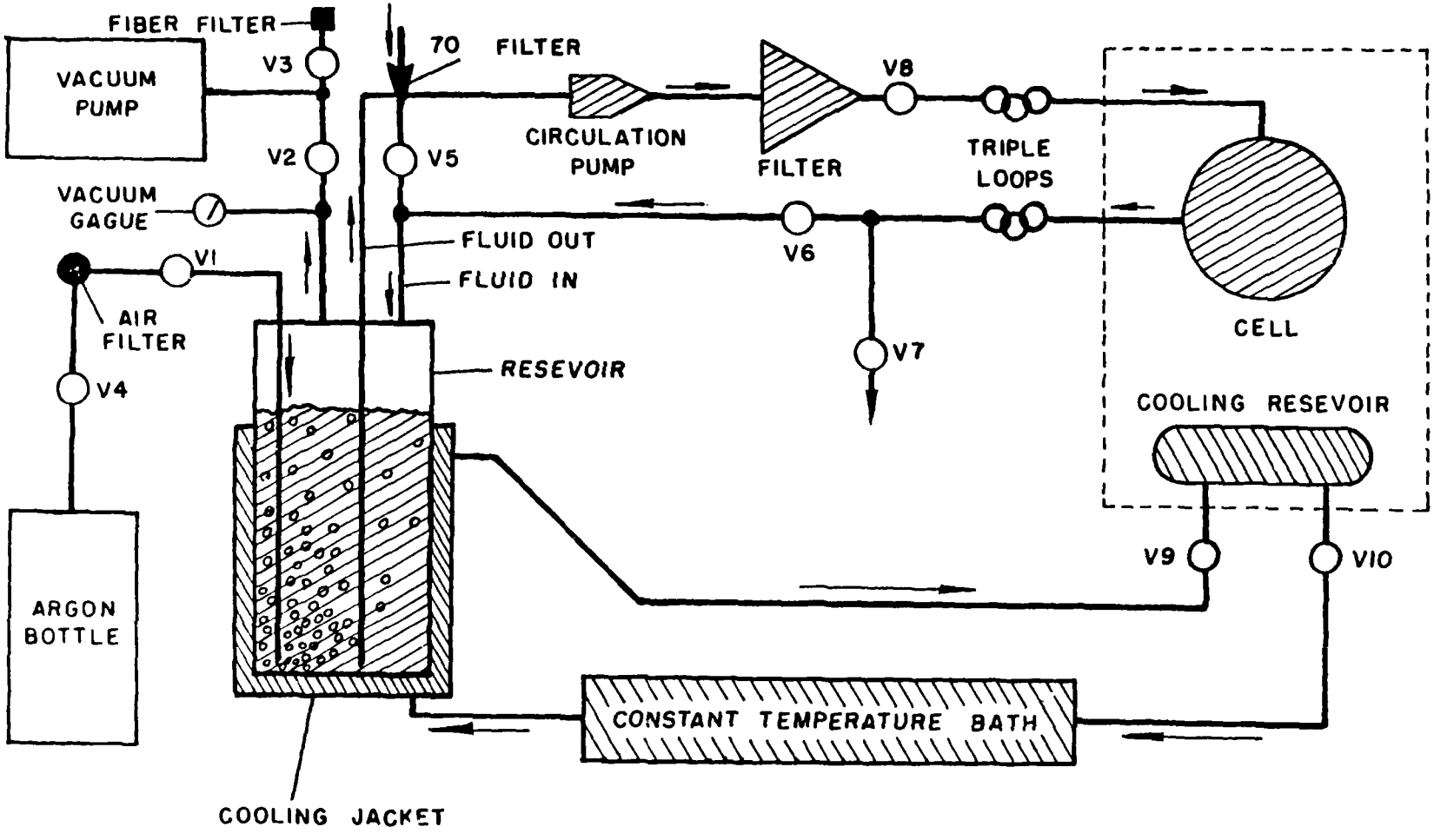

FIG. XV FLUID MANAGEMENT SYSTEM

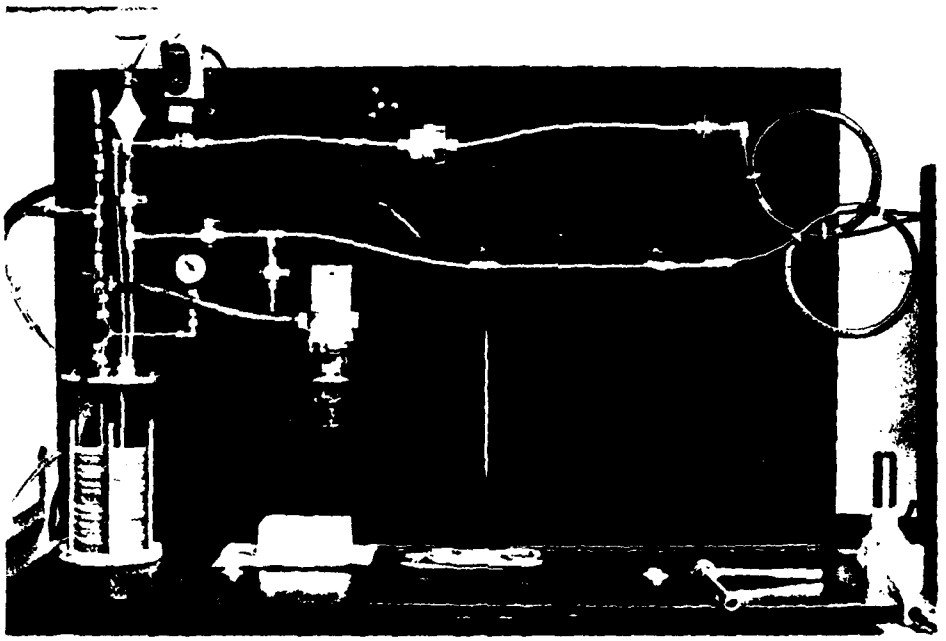

FIG. XVI FILTRATION SYSTEM PHOTOGRAPH

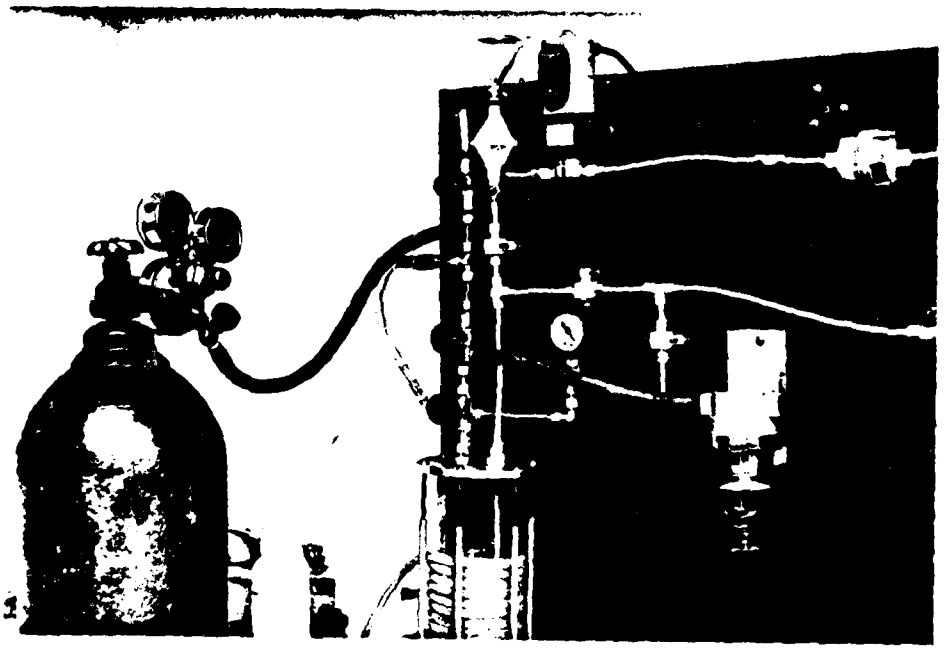

FIG. XVII DEGASSING SYSTEM PHOTOGRAPH

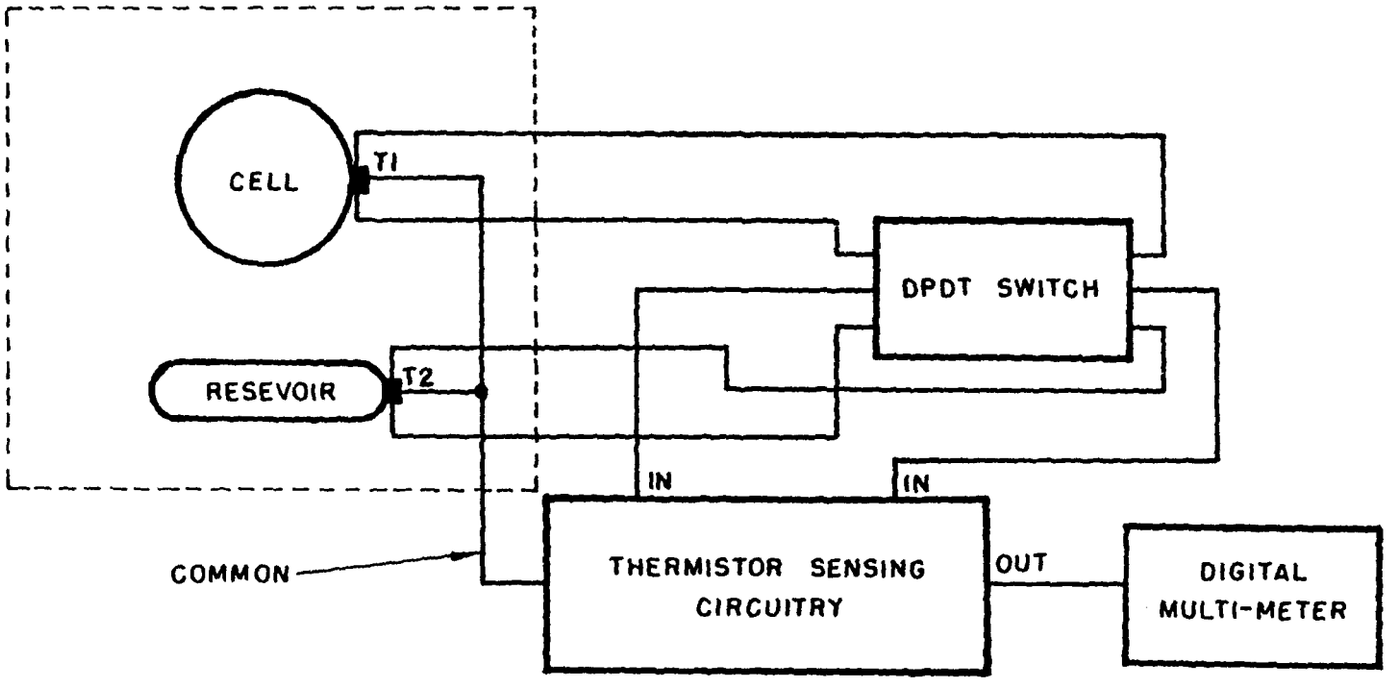

FIG. XVIII TEMPERATURE MONITORING SYSTEM

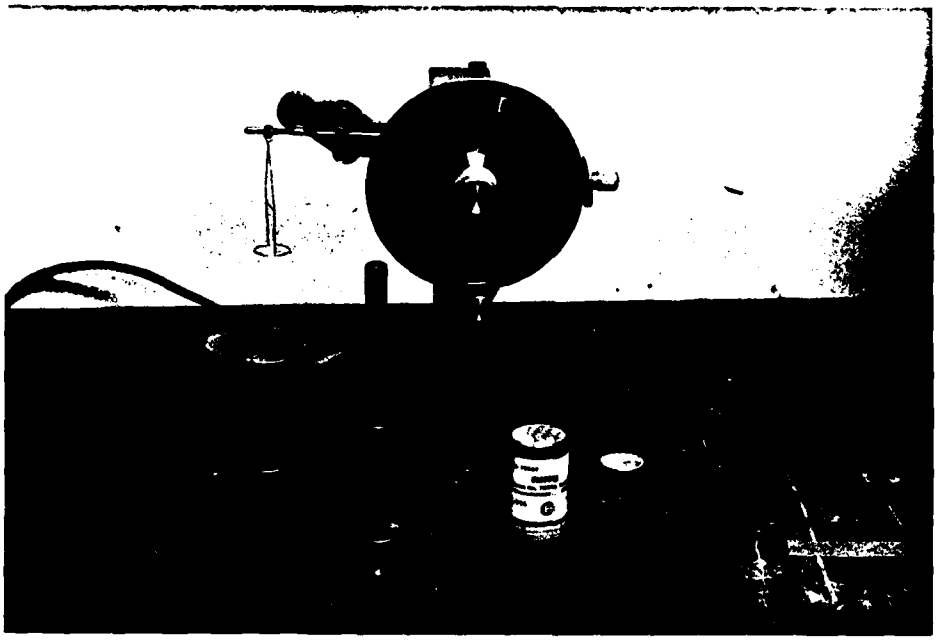

FIG. XIX TENSIOMETER PHOTOGRAPH

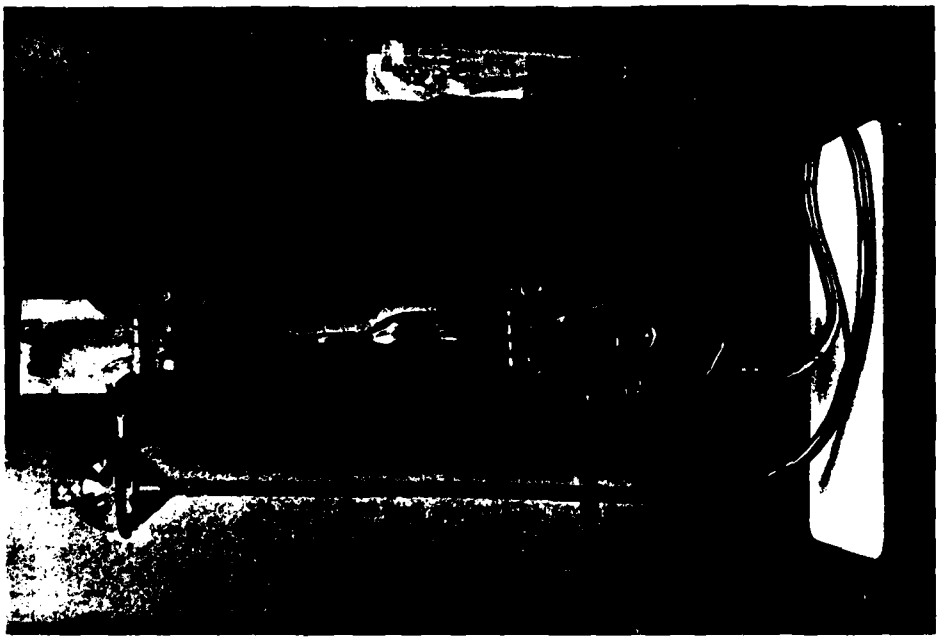

FIG. XX VAN SLYKE APPARATUS PHOTOGRAPH

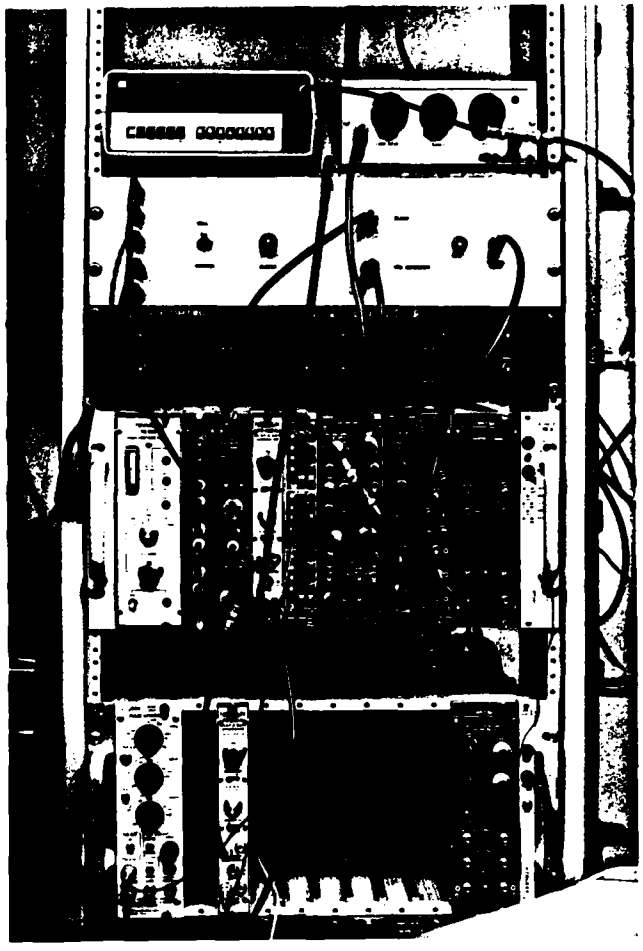

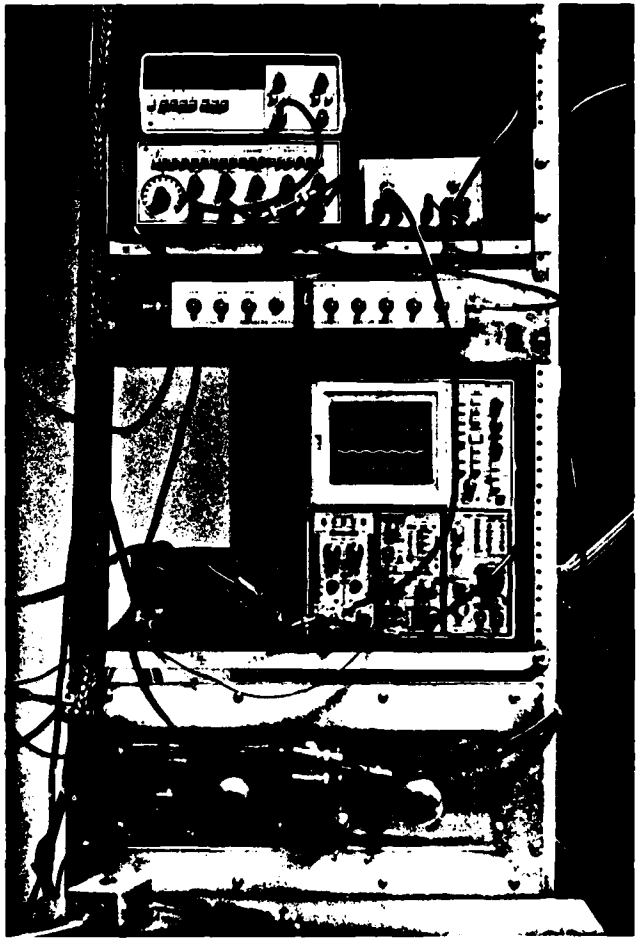

FIG XXI SYSTEM ELECTRONICS PHOTOGRAPHS

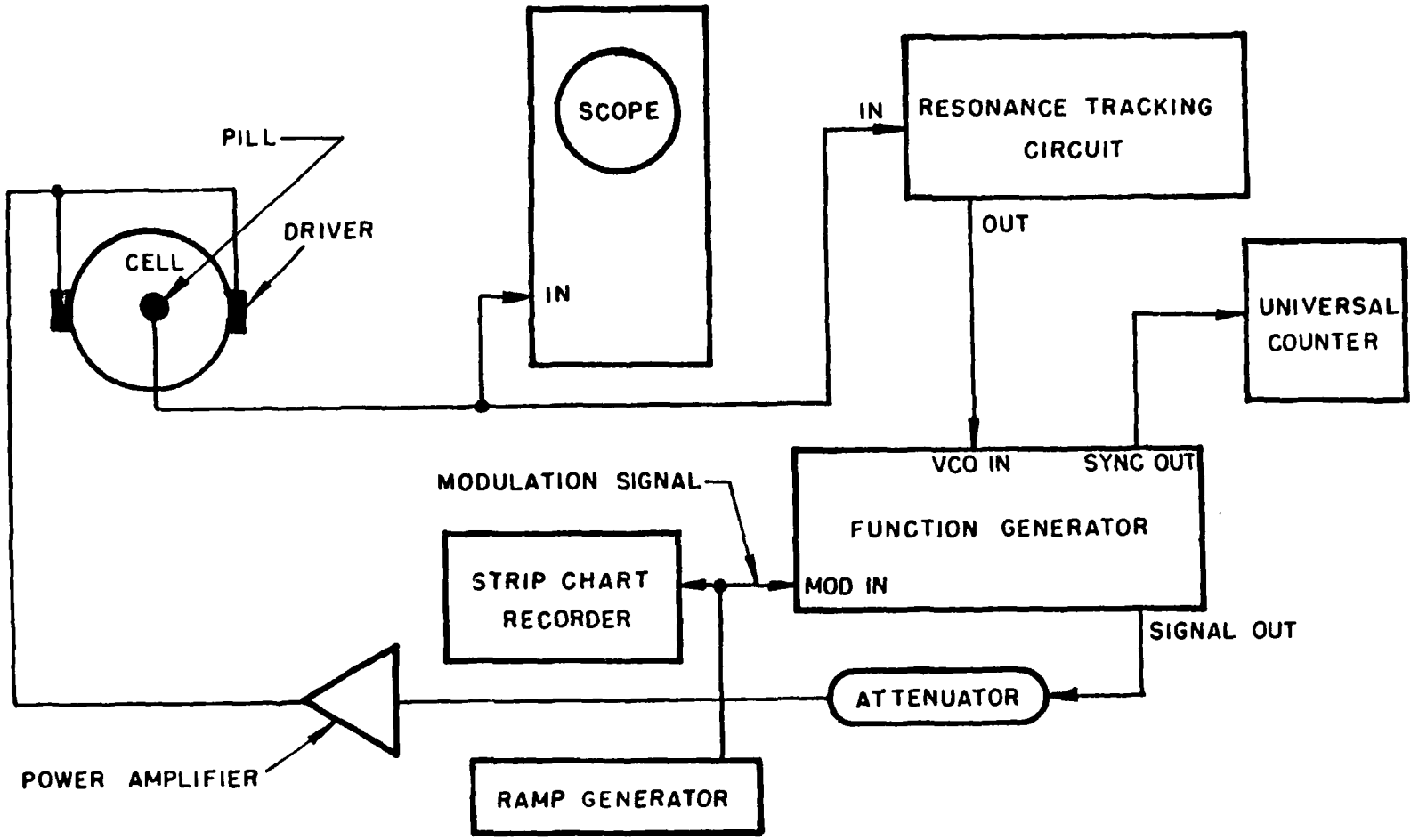

FIG. XXII POWER AND FREQUENCY CONTROL CIRCUITRY

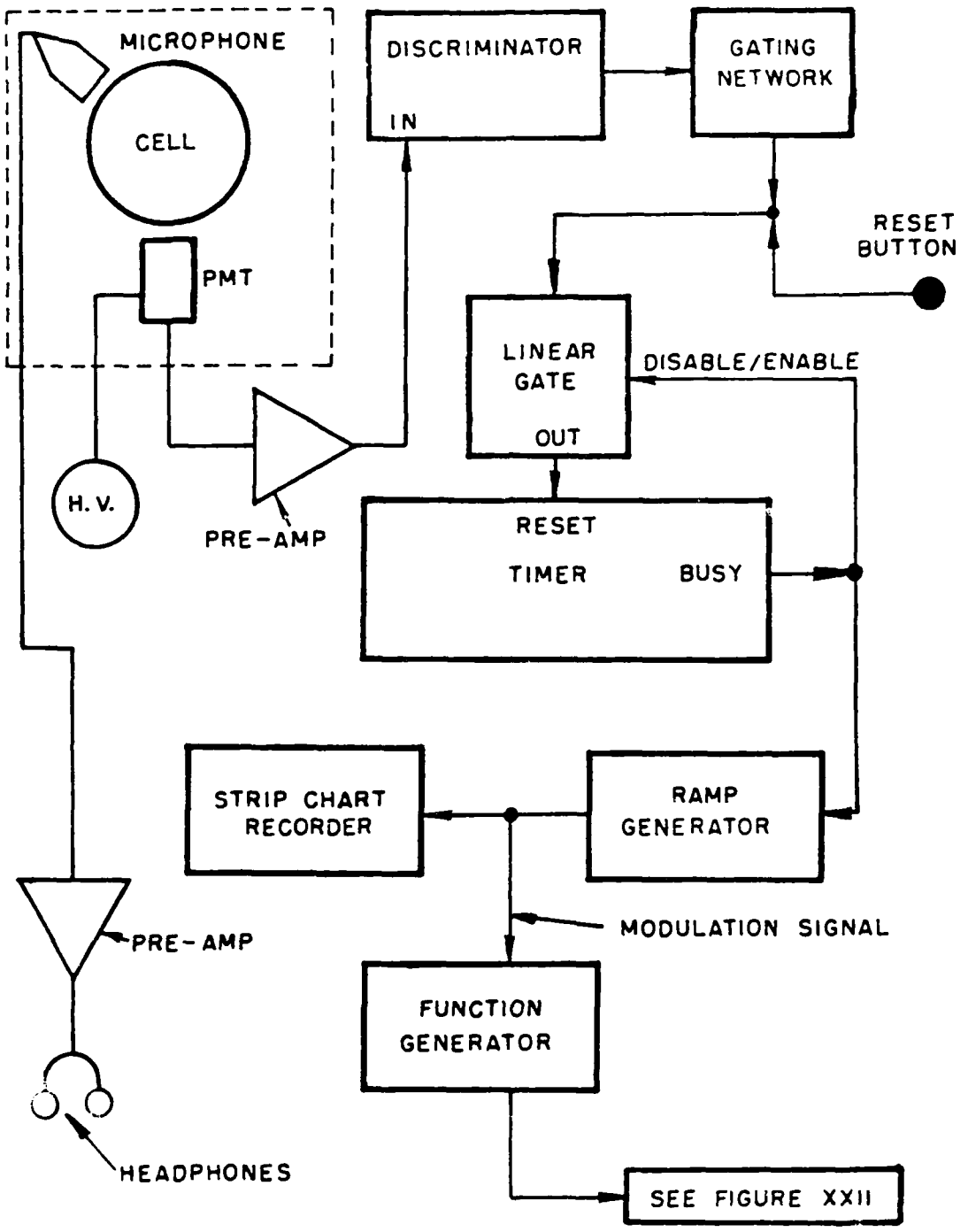

FIG. XXIII GATING, TRIGGERING, TIMING

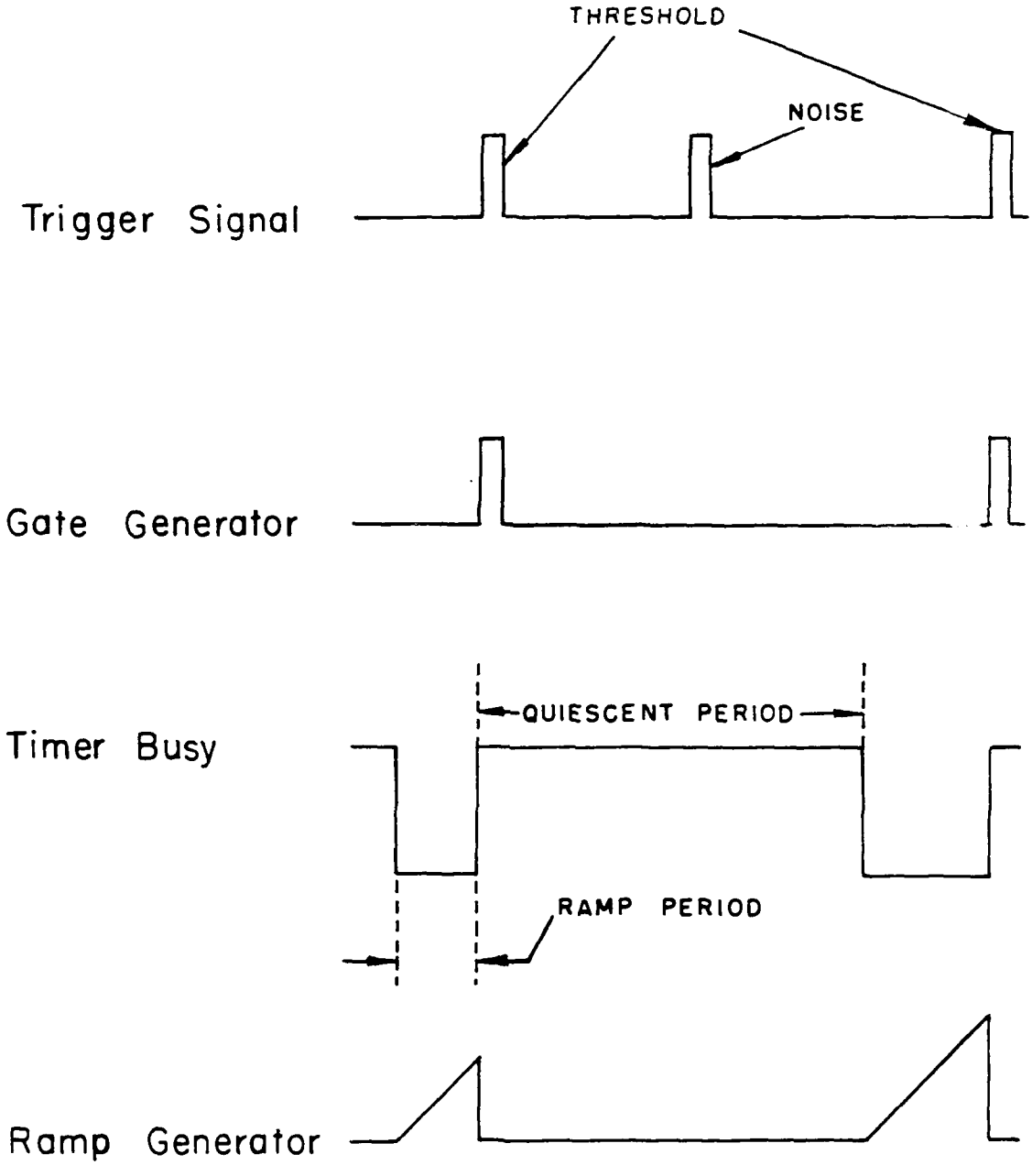

FIG. XXIV TIMING CHARACTERISTICS

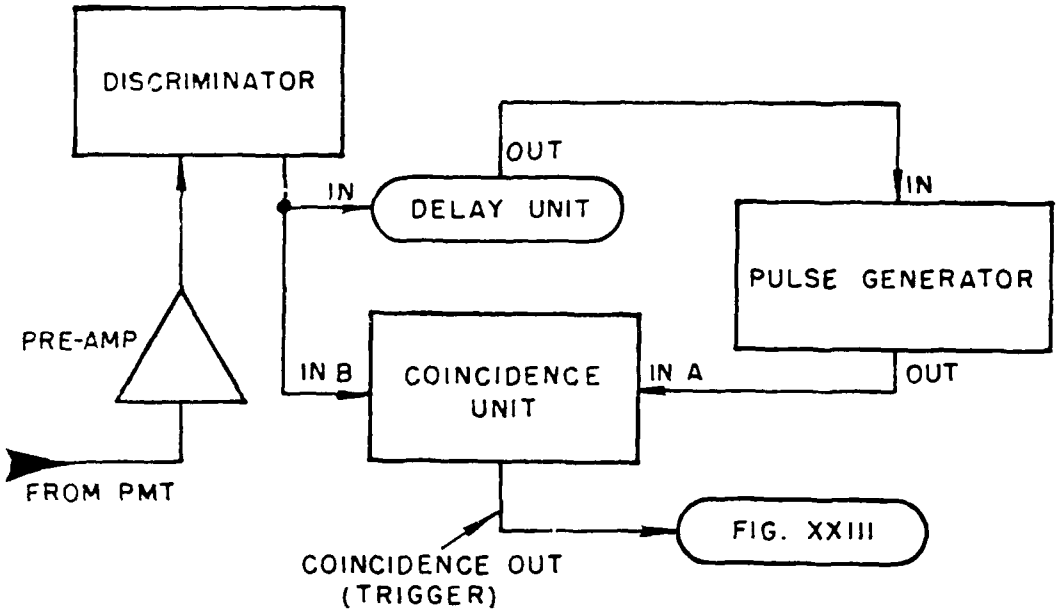

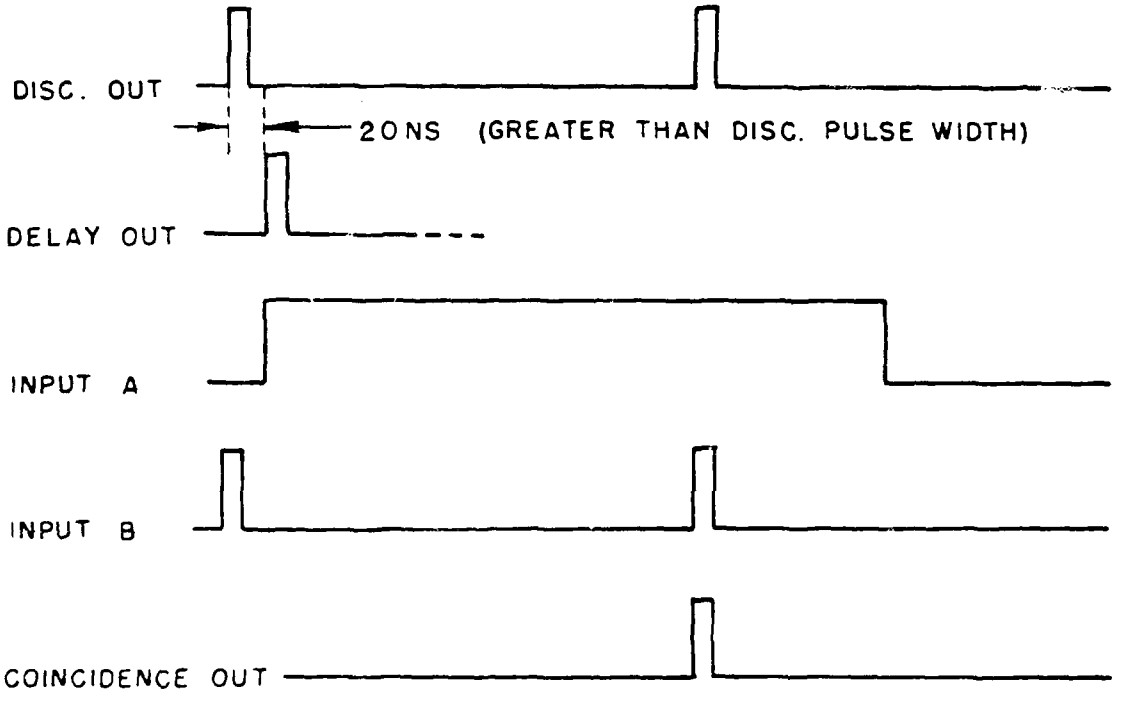

FIG. XXV GATING NETWORK

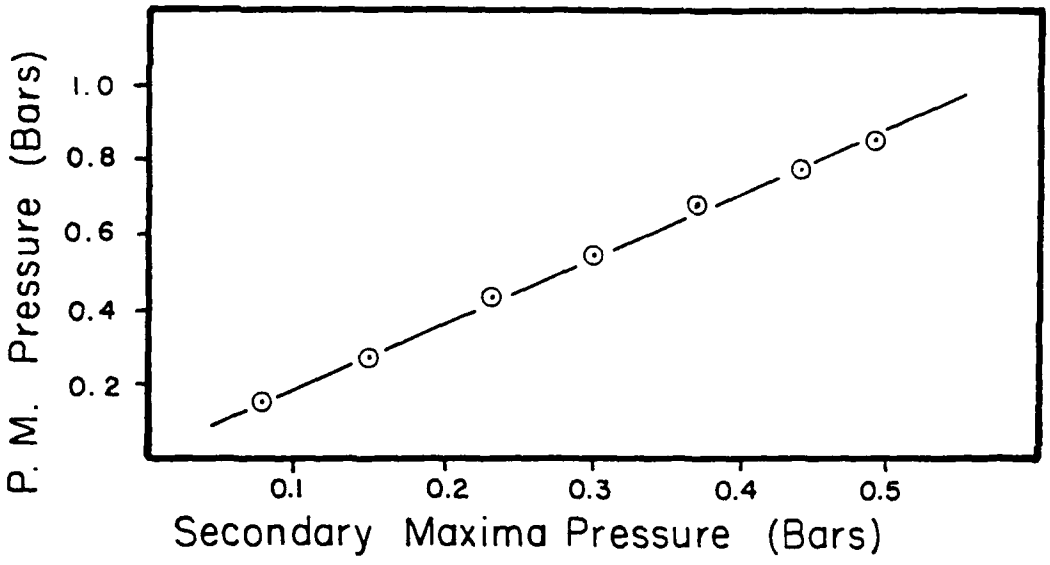

FIG. XXVI PRIMARY VS. SECONDARY MAXIMA

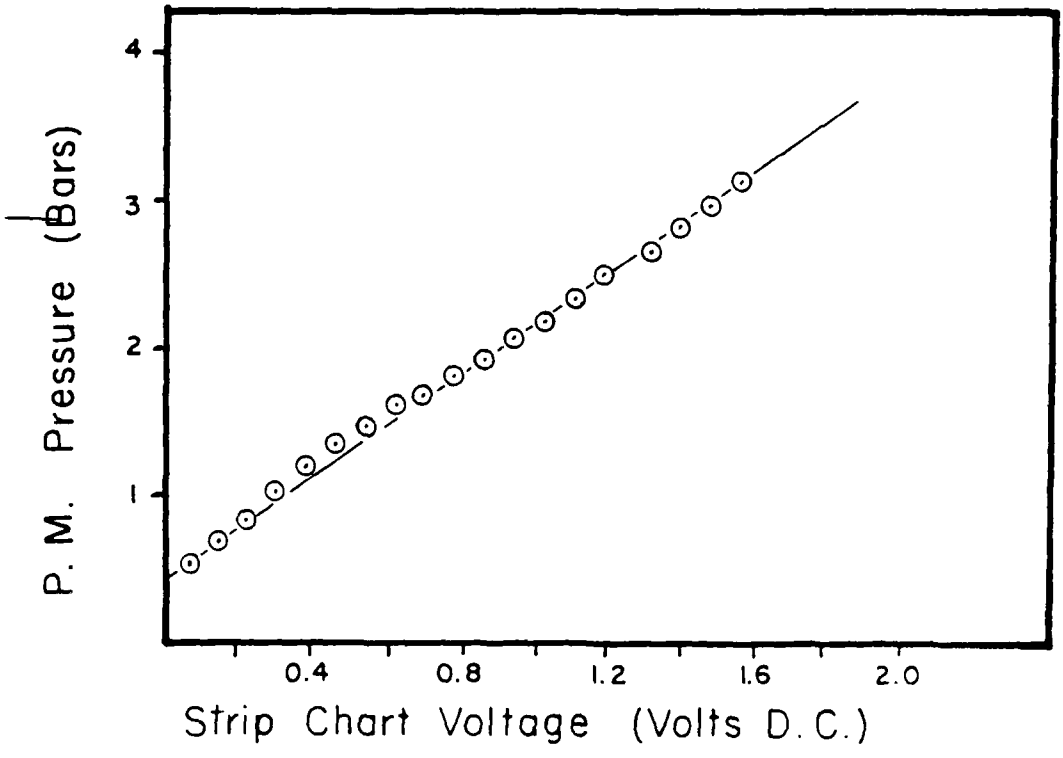

FIG. XXVII SYSTEM CALIBRATION CURVE

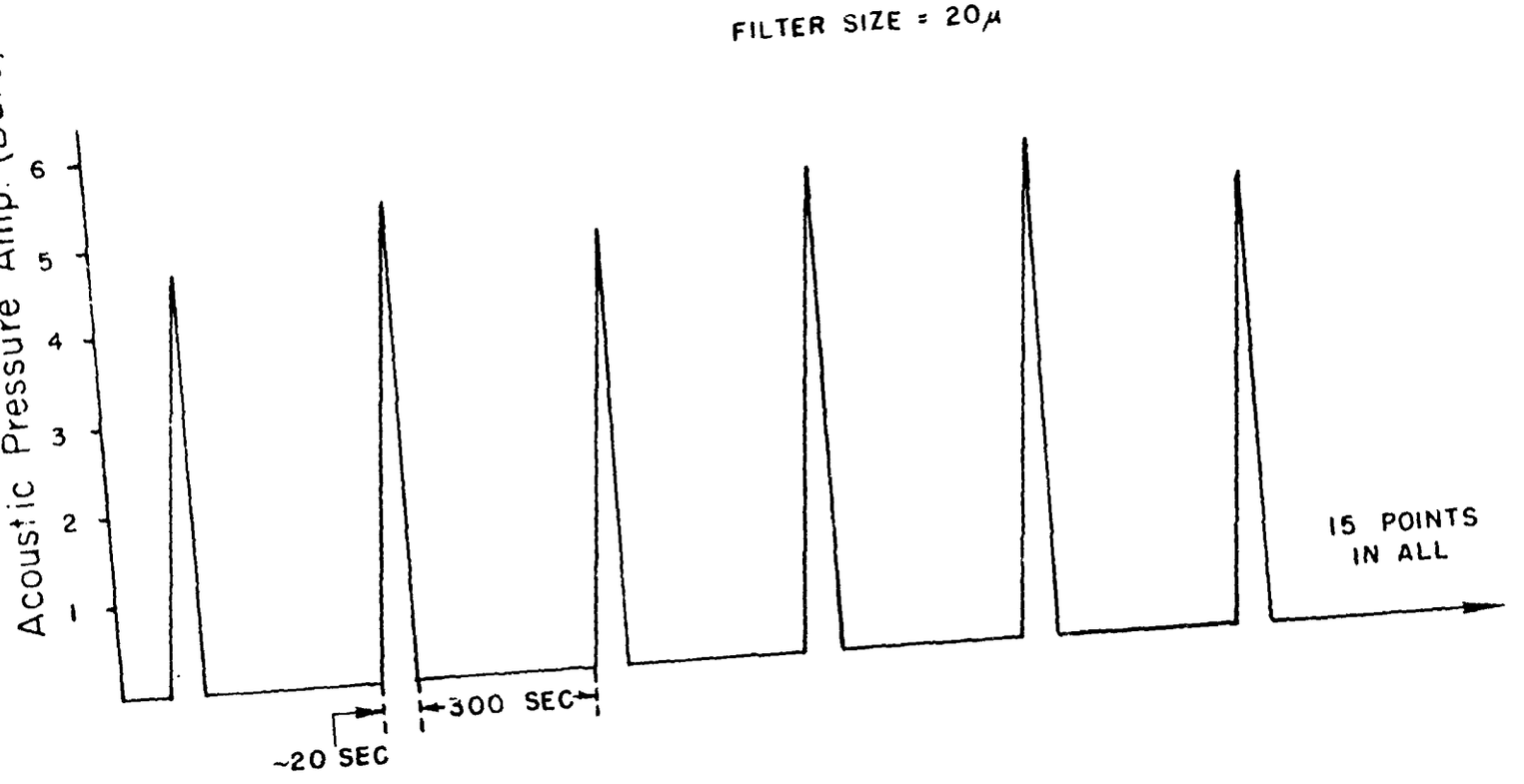

FIG. XXVIII SAMPLE STRIP CHART RECORD (SIMULATED)

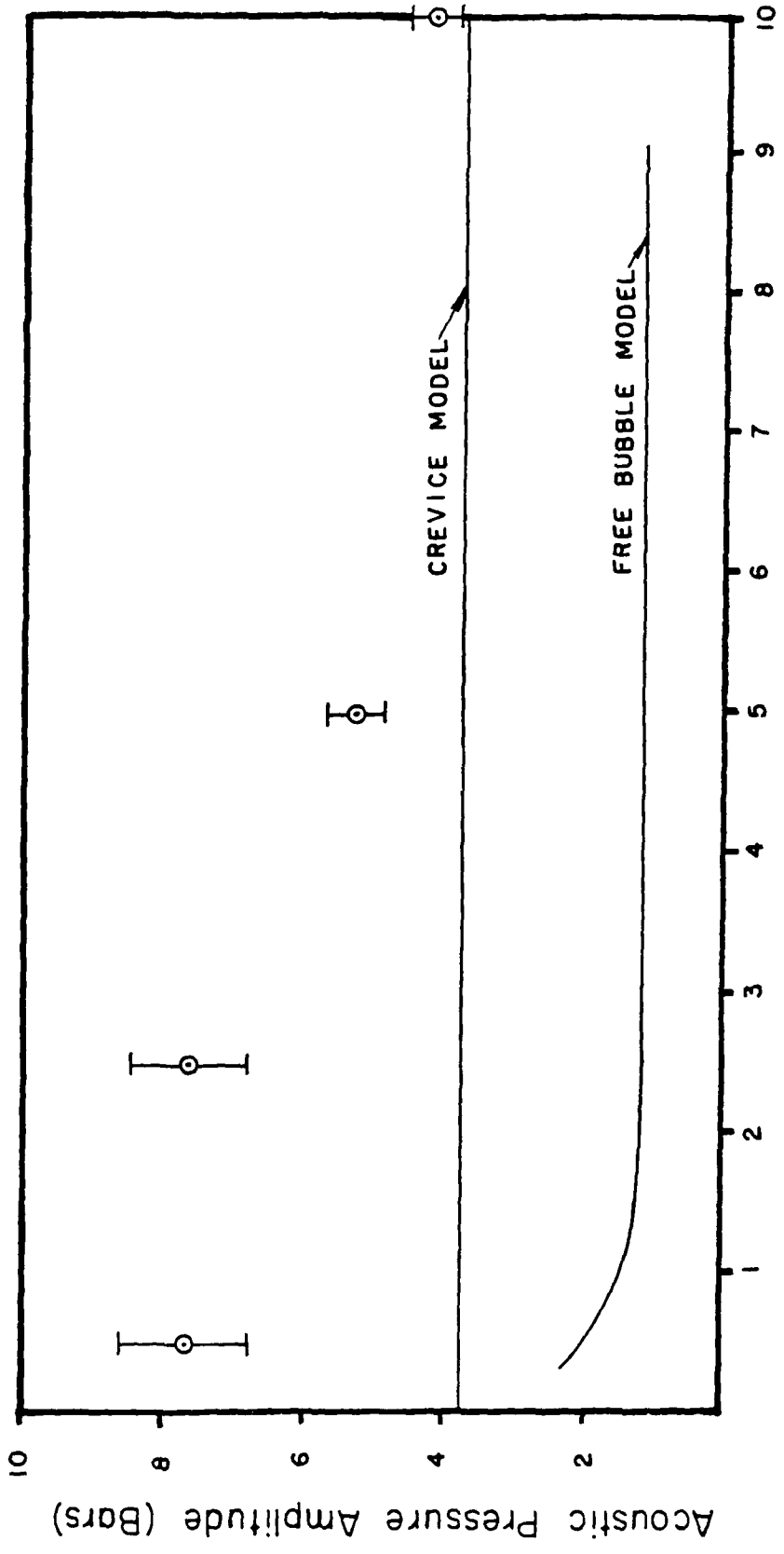

FIG. XXIX EXPERIMENTAL RESULTS

BIOGRAPHICAL SKETCH OF THE AUTHOR

Ronald Aurele Roy, son of Aurele and Lucienne Roy, was born on December 10, 1956 in Lewsiton, Maine. He attended the University of Maine in Orono, Maine, and graduated with Highest Distinction with a B.S. in Engineering Physics in 1981. He is presently enrolled in a Ph.D program in Applied Mechanics at Yale University. Ronald Roy is a member of Sigma Pi Sigma, Tau Beta Pi, Phi Kappa Phi, the American Physical Society, the Audio Engineering Society, and the Acoustical Society of America. He has been an NSF-URP fellow and is currently an ONR fellow. He has worked as a research assistant, laboratory instructor, design technician, tutor, television camera-person, sound engineer, painter, factory worker, etc.. Ronald Roy plans to persue a career in physics research and is presently living with his wife, Nancy, and child, Caitlyn, at 511 Prospect Street, Apartment 2, New Haven, Connecticut, 06511.

February 1983

REPORTS DISTRIBUTION LIST FOR ONR PHYSICS DIVISION OFFICE
UNCLASSIFIED CONTRACTS

Director Defense Advanced Research Projects Agency Attn: Technical Library 1400 Wilson Blvd. Arlington, Virginia 22209	3 copies
Office of Naval Research Physics Division Office (Code 412) 800 North Quincy Street Arlington, Virginia 22217	3 copies
Office of Naval Research Director, Technology (Code 200) 800 North Quincy Street Arlington, Virginia 22217	1 copy
Naval Research Laboratory Department of the Navy Attn: Technical Library Washington, DC 20375	3 copies
Office of the Director of Defense Research and Engineering Information Office Library Branch The Pentagon Washington, DC 20301	3 copies
U. S. Army Research Office Box 1211 Research Triangle Park North Carolina 27709	2 copies
Defense Technical Information Center Cameron Station Alexandria, Virginia 22314	12 copies
Director, National Bureau of Standards Attn: Technical Library Washington, DC 20234	1 copy
Commanding Officer Office of Naval Research Western Detachment Office 1030 East Green Street Pasadena, California 91101	3 copies
Commanding Officer Office of Naval Research Eastern/Central Detachment Office 495 Summer Street Boston, Massachusetts 02210	3 copies

Commandant of the Marine Corps
Scientific Advisor (Code RD-1)
Washington, DC 20380 — 1 copy

Naval Ordnance Station
Technical Library
Indian Head, Maryland 20640 — 1 copy

Naval Postgraduate School
Technical Library (Code 0212)
Monterey, California 93940 — 1 copy

Naval Missile Center
Technical Library (Code 5632.2)
Point Mugu, California 93010 — 1 copy

Naval Ordance Station
Technical Library
Louisville, Kentucky 40214 — 1 copy

Commanding Officer
Naval Ocean Research & Development Activity
Technical Library
NSTL Station, Mississippi 39529 — 1 copy

Naval Explosive Ordnance Disposal Facility
Technical Library
Indian Head, Maryland 20640 — 1 copy

Naval Ocean Systems Center
Technical Library
San Diego, California 92152 — 1 copy

Naval Surface Weapons Center
Technical Library
Silver Spring, Maryland 20910 — 1 copy

Naval Ship Research and Development Center
Central Library (Code L42 and L43)
Bethesda, Maryland 20084 — 1 copy

Naval Avionics Facility
Technical Library
Indianapolis, Indiana 46218 — 1 copy